Recent cryovolcanism in Virgil Fossae on Pluto

Dale P Cruikshank, Orkan M Umurhan, Ross A Beyer, B Schmitt, James T Keane, Kirby D Runyon, Dimitra Atri, Oliver L White, Isamu Matsuyama, Jeffrey M Moore, et al.

Recent Cryovolcanism in Virgil Fossae on Pluto

Revised April 19, 2019

Dale P. Cruikshank*[a], Orkan M.Umurhan[a], Ross A. Beyer[a], Bernard Schmitt[b], James T. Keane[c], Kirby D. Runyon[d], Dimitra Atri[e,f], Oliver L. White[a], Isamu Matsuyama[g], Jeffrey M. Moore[a], William B. McKinnon[h], Scott A. Sandford[a], Kelsi N. Singer[i], William M. Grundy[j], Cristina M. Dalle Ore[a,k], Jason C. Cook[l], Tanguy Bertrand[a], S. Alan Stern[i], Catherine B. Olkin[i], Harold A. Weaver[d], Leslie A. Young[i], John R. Spencer[i], Carey M. Lisse[d], Richard P. Binzel[m], Alissa M. Earle[m], Stuart J. Robbins[i], G. Randall Gladstone[n], Richard J. Cartwright[a,k], Kimberly Ennico[a],

*Corresponding author
[a]NASA Ames Research Center, Moffett Field, CA, United States
[b]Université Grenoble Alpes, CNRS, IPAG, Grenoble, France
[c]California Institute of Technology, Pasadena, CA, United States
[d]Applied Physics Laboratory, Johns Hopkins University, Laurel, MD, United States
[e]New York University Abu Dhabi, Abu Dhabi, United Arab Emirates
[f]Blue Marble Space Institute, Seattle, WA, United States
[g]Lunar and Planetary Laboratory, University of Arizona, Tucson, AZ, United States
[h]Washington University, St. Louis, MO, United States
[i]Southwest Research Institute, Boulder, CO, United States
[j]Lowell Observatory, Flagstaff, AZ, United States
[k]SETI Institute, Mountain View, CA, United States
[l]Pinhead Institute, Telluride, CO, United States
[m]Massachusetts Institute of Technology, Cambridge, MA, United States
[n]Southwest Research Institute, San Antonio, TX, United States

Additional author information:

Dale P. Cruikshank
MS 246-6
NASA Ames Research Center
Moffett Field, CA 94035
Dale.P.Cruikshank@nasa.gov
650-604-1444
FAX 650-604-6779

Umurhan, Orkan M.
MS 246-3
NASA Ames Research Center
Moffett Field, CA 94035
Orkan.M.Umurhan@nasa.gov
650-604-5000

J. M. Moore
MS 246-3
NASA Ames Research Center
Moffett Field, CA 94035
Jeff.Moore@nasa.gov
60-604-5529

W. M. Grundy
Lowell Observatory
1400 W. Mars Hill Rd.
Flagstaff, AZ 86001
w.grundy@lowell.edu

S. A. Stern
Southwest Research Institute
1050 Walnut St. Ste. 400
Boulder, CO 80302
alan@boulder.swri.edu
303-546-9670

C. B. Olkin
Southwest Research Institute
1050 Walnut St.
Boulder, CO 80302
colkin@boulder.swri.edu
303-546-9670

L. A. Young
Southwest Research Institute
1050 Walnut St.
Boulder, CO 80302
layoung@boulder.swri.edu
303-546-9670

K. Ennico
NASA Ames Research Center
Moffett Field, CA 94035
Kimberly.Ennico@nasa.gov
650-604-6067

H. A. Weaver
Applied Physics Lab.
Johns Hopkins University
Laurel, MD
Hal.Weaver@JHUAPL.edu
443-778-8078

C. M. Dalle Ore
MS 245-6
NASA Ames Research Center
Moffett Field, CA 94035
650-604-6151
Cristina.M.Dalleore@nasa.gov
650-604-6151

C. M. Lisse
Applied Physics Lab.
Johns Hopkins University
Laurel, MD
Carey.Lisse@jhuapl.edu
240-228-0535

K. D. Runyon
Applied Physics Lab.
Johns Hopkins University
Laurel, MD
Kirby.Runyon@jhuapl.edu
443-778-5000

R. A. Beyer
MS 245-3
NASA Ames Research Center
Moffett Field, CA 94035
Ross.a.beyer@nasa.gov
650-604-0324

B. Schmitt
Université Grenoble Alpes
CNRS, IPAG
Grenoble, France F-38000
bernard.schmitt@univ-grenoble-alpes.fr

Richard J. Cartwright
SETI Institute
189 N. Bernardo Ave., Ste 200
Mountain View, CA 94043
rcartwright@seti.org

Dimitra Atri
New York University Abu Dhabi
Saadiyat Island, Abu Dhabi
United Arab Emirates

da99@nyu.edu

Isamu Matsyuama
Lunar and Planetary Lab.
University of Arizona
Tucson, AZ 85721
isa@lpl.arizona.edu

John Spencer
Southwest Research Institute
1050 Walnut St.
Boulder, CO 80302
spencer@boulder.swri.edu
303-546-9670

G. Randall Gladstone
Southwest Research Institute
6220 Culebra Rd.
San Antonio, TX 78238
rgladstone@swri.edu

James T. Keane
California Institute of Technology
Pasadena, CA 91125
jkeane@caltech.edu
626-395-4241

Oliver L. White
MS 245-3
NASA Ames Research Institute
Moffett Field, CA 94035
oliver.l.white@nasa.gov

Scott A. Sandford
MS 245-6
NASA Ames Research Institute
Moffett Field, CA 94035
Scott.A.Sandford@nasa.gov

Wm. B. McKinnon
Washington University
St. Louis, MO
mckinnon@wustl.edu

Jason C. Cook
Pinhead Institute

Telluride, CO
jccook@boulder.swri.edu

T. Bertrand
MS 245-3
NASA Ames Research Institute
Moffett Field, CA 94035
Tanguy.Bertrand@nasa.gov
650-537-5334

Richard P. Binzel
Massaschusetts Institute of Technology
Cambridge, MA
rpb@mit.edu

Alissa M. Earle
Massaschusetts Institute of Technology
Cambridge, MA
aearle@mit.edu

Stuart Robbins
Southwest Research Institute
1050 Walnut St.
Boulder, CO 80302
303-546-9670
stuart@boulder.swri.edu

Kelsi N. Singer
Southwest Research Institute
1050 Walnut St.
Boulder, CO 80302
303-546-9670
kelsi.singer@gmail.com

Key Words

-Pluto, surface
-Ices, IR spectroscopy
-Interiors
-Organic chemistry
-Volcanism

Highlights

•A tectonic structure (Virgil Fossae) on Pluto may be a source of a cryolava that has been erupted onto the planet's surface.

•The putative cryolava consists primarily of H_2O, but it carries the spectral signature of ammonia (NH_3), which may occur as an ammonia hydrate or an ammoniated salt. It also carries a distinctively colored component thought to be complex organic matter (a tholin).

•Because NH_3 in its various forms is susceptible to destruction by UV photons and charged particles, its presence suggests emplacement on Pluto's surface sometime in the past billion years.

•In addition to the debouchment of cryolava along fault lines in Virgil Fossae, fountaining from one or more associated sites appears to have distributed a mantling layer covering a few thousand square kilometers.

•The planet-scale geophysical setting of Virgil Fossae in a large region stressed by factors related to the nitrogen glacier Sputnik Planitia is consistent with extensional fracturing. Some fractures appear to have facilitated the emergence of a cryolava from one or more reservoirs in the subsurface.

Abstract

The Virgil Fossae region on Pluto exhibits three spatially coincident properties that are suggestive of recent cryovolcanic activity over an area approximately 300 by 200 km. Situated in the fossae troughs or channels and in the surrounding terrain are exposures of H_2O ice in which there is entrained opaque red-colored matter of unknown composition. The H_2O ice is also seen to carry spectral signatures at 1.65 and 2.2 μm of NH_3 in some form, possibly as a hydrate, an ammoniated salt, or some other compound. Model calculations of NH_3 destruction in H_2O ice by galactic cosmic rays suggest that the maximum lifetime of NH_3 in the uppermost meter of the exposed surface is ~10^9 years, while considerations of Lyman-α ultraviolet and solar wind charged particles suggest shorter timescales by a factor of 10 or 100. Thus, 10^9 y is taken as an upper limit to the age of the emplacement event, and it could be substantially younger.

The red colorant in the ammoniated H_2O in Virgil Fossae and surroundings may be a macromolecular organic material (tholin) thought to give color to much of Pluto's surface, but probably different in composition and age. Owing to the limited spectral range of the New Horizons imaging spectrometer and the signal precision of the data, apart from the H_2O and NH_3 signatures there are no direct spectroscopic clues to the chemistry of the strongly colored deposit on Pluto. We suggest that the colored material was a component of the fluid reservoir from which the material now on the surface in this region was erupted. Although other compositions are possible, if it is indeed a complex organic material it may incorporate organics inherited from the solar nebula, further processed in a warm aqueous environment inside Pluto.

A planet-scale stress pattern in Pluto's lithosphere induced by true polar wander, freezing of a putative interior ocean, and surface loading has caused fracturing in a broad arc west of Sputnik Planitia, consistent with the structure of Virgil Fossae and similar extensional features. This faulting may have facilitated the ascent of fluid in subsurface reservoirs to reach the surface as flows and as fountains of cryoclastic materials, consistent with the appearance of colored, ammoniated H_2O ice deposits in and around Virgil Fossae. Models of a cryoflow emerging from sources in Virgil Fossae indicate that the lateral extent of the flow can be several km (Umurhan et al. 2019). The deposit over the full length (>200 km) of the main trough in the Virgil Fossae complex and extending through the north rim of Elliot crater and varying in elevation over a range of ~2.5 km, suggests that it debouched from multiple sources, probably along the length of the strike direction of the normal faults defining the graben. The source or sources of the ammoniated H_2O are one or more subsurface reservoirs that may or may not connect to the global ocean postulated for Pluto's interior. Alternatives to cryovolcanism in producing the observed characteristics of the region around Virgil Fossae are explored in the discussion section of the paper.

1. Introduction

New understanding of the geologic structures and surface processes on Pluto is emerging from the continued scrutiny and analysis of the images obtained with the New Horizons spacecraft at the July 14, 2015 flyby, building on the early work presented by Moore et al. (2016, 2017), Schenk (2018) and others. Similarly, study of compositional maps of the surface derived from the Linear Etalon Imaging Spectral Array (LEISA) instrument, following on the early papers (Grundy et al. 2016a, Protopapa et al. 2017, Schmitt et al. 2017), reveals more detailed information about the geographic distribution of various surface components and their interactions. Information on the New Horizons mission, the spacecraft and instruments, and early science results is given in Stern et al. (2015). In this paper we examine the region along the northern margin of a region of large spatial extent informally called Cthulhu and that includes Virgil Fossae, Elliot crater, and other structures in the context of the recent detection of NH_3 (possibly as a hydrate $NH_3 \bullet nH_2O$ or an ammoniated salt) and its spatial correlation with a prominent exposure of H_2O ice in this region (Dalle Ore et al. 2019; Cruikshank et al. 2019).

Water ice is regarded as the bedrock of Pluto's surface because of its rigidity and its exceedingly low vapor pressure at the ambient temperature of ~40-45 K. Water is the presumed most abundant non-silicate component of Pluto's interior, and while it is presently frozen solid at the surface forming a crust of unknown thickness, it may be liquid at depth (Nimmo et al. 2016). It is upon this crustal bedrock that layers of much more volatile ices, predominantly N_2, CH_4, and CO, are distributed in patterns regulated by exchange with the atmosphere and molecular migration governed by their individual vapor pressure dependence on temperature and Pluto's short- and long-term seasons (Earle et al. 2017). Water ice is exposed in various regions of Pluto's surface, notably at Virgil Fossae, Pulfrich crater, and the whole of Cthulhu (Schmitt et al. 2017; Cook et al. 2018), although the spectral signature is muted in some instances by the color and albedo

of the surroundings. Surface modification by volatile transport or more aggressive processes such as impacts (Singer et al. 2019; Robbins et al. 2017) and glaciation (Umurhan et al. 2017, Howard et al. 2017) may uncover bedrock H_2O ice locally.

In addition to geological processes thus far identified in published works, there are other structures and surface regions on Pluto that suggest the emergence of fluids from the subsurface, for example at Wright and Piccard Montes (Singer et al. 2016) and possibly elsewhere in the broad arc west of Sputnik Planitia that includes Virgil Fossae and extends from the equator to ~60° N. latitute (Schenk et al. 2018), In the present paper we explore the region in and around Virgil Fossae both from structural and compositional viewpoints, and conclude that there is a strong case for cryovolcanic activity in Pluto's past ~1 billion years. We first examine the geological and geographical setting of Virgil Fossae, and then the composition of the ices found therein. One ice component, NH_3, is susceptible to destruction by factors in the space environment, and its persistence argues for relatively recent emplacement or exposure to view. Those environmental factors are explored in some detail, with the conclusion that it is unlikely that the NH_3 spectral signature could survive on the surface from the time of Pluto's formation in the outer Solar System. Similarly, we inquire into the chemistry and origin of the unique coloration of parts of the Virgil Fossae structure, and conclude that the colored material most likely emerged from a fluid reservoir at some unknown depth in the planet's crust. The process by which this fluid emerged on the surface is suggested to have had two components. The first component arises from fluid debouchment along the fractures defining the Virgil Fossae main trough, which is a graben resulting from extentional tectonics in this region of the planet. The second appears to be a deposit distributed over an area of a few thousand square kilometers by one or more fountaining events, which may or may not have been contemporaneous.

Alternatives to cryovolcanism in producing the observed characteristics of the region around Virgil Fossae are briefly explored in the discussion section of the paper.

2. Virgil Fossae

2.1 Geological and geographical setting

Virgil Fossae is a prominent graben complex on the northern edge of the dark-brown colored and geologically ancient Cthulhu (Figure 1). The set of graben likely formed from a combination of extensional stresses, including stresses arising from the global expansion of Pluto due to the freezing of a subsurface ocean (Stern et al. 2015; Hammond et al. 2016; Moore et al. 2016), stresses arising from the loading of the Sputnik Planitia to the east (Keane et al. 2016), and stresses caused by the resulting reorientation (true polar wander) of Pluto after the formation of Sputnik Planitia (Nimmo et al. 2016; Keane et al. 2016). The combination of loading and reorientation stresses accurately predicts the SW-NE orientation of Virgil Fossae (Keane et al. 2016).

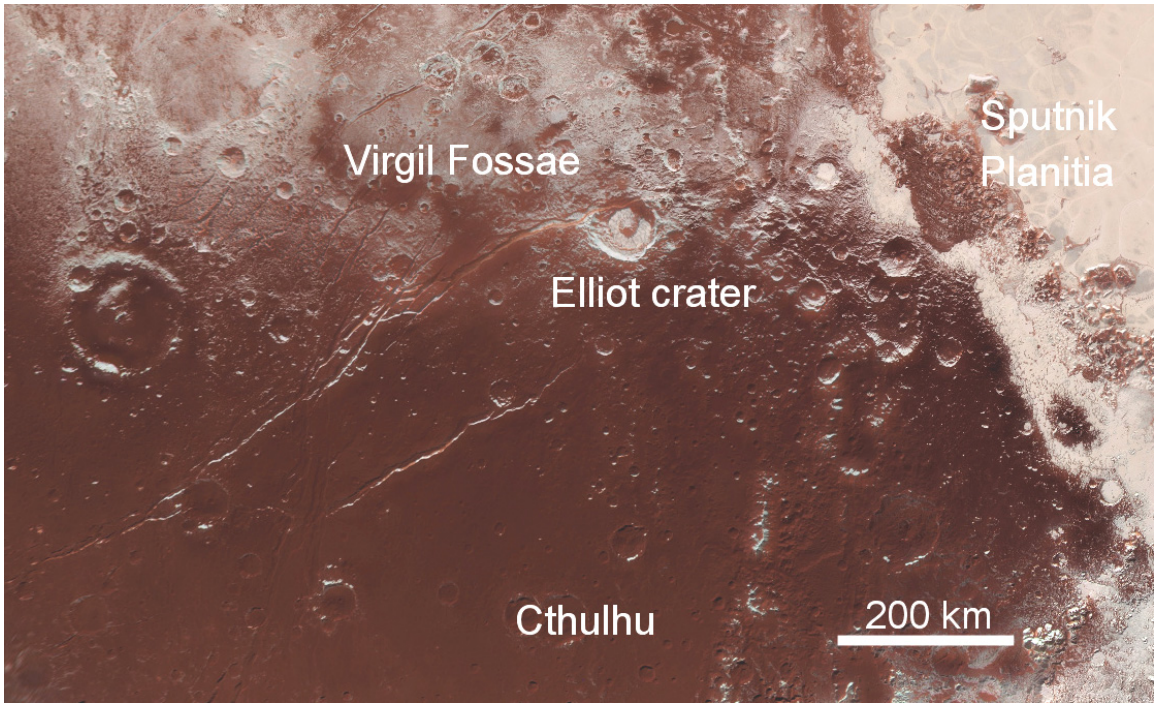

Figure 1. Multispectral Visible Imaging Camera (MVIC) image of Cthulhu and the surrounding terrain southwest of Sputnik Planitia, with the color artifically enhanced to show contrasts in the albedo and color differences in the geological and geographical structures across the planet.

The dark-brown region informally called Cthulhu spans an equatorial zone ranging from ~15°N to ~20°S, wrapping around ~1/3 of the circumference of Pluto, from ~20°E to ~160°E (Moore et al. 2016). This region of varied topography and geological terrains appears to be mantled by a layer of red-brown, low-albedo material. While this mantling is generally thin enough to preserve many underlying structures (e.g., dendritic valleys, craters, fossae, etc.; Moore et al. 2016), the notable lack of craters in this region may indicate that the layering is locally thick enough to remove or obscure some craters, or that some other resurfacing process is active (Singer et al. 2016; Robbins et al. 2017). The dark, red-brown color likely results from ultraviolet and/or charged particle photolysis/radiolysis of atmospheric gases and/or surface ices. When methane and molecular nitrogen are exposed to energetic photons and particles, they are converted to complex organic molecules with colors ranging from yellow to red and dark brown (Imanaka et al. 2004; Cruikshank et al. 2005; Materese et al. 2014, 2015). This is discussed more below.

While Cthulhu is characterized by dark, red-brown material, it is clear in the enhanced color image (Figure 1) that the color of the terrain around Virgil Fossae is different. The largest graben trough of Virgil Fossae, which cuts through the northern rim of Elliot crater, is surrounded by lighter, orange-colored material. The main trough of the Virgil Fossae complex extends approximately east-west for nearly 300 km, and then beyond in a series of en echelon fractures with strike-slip components. The main trough varies in width over its course and at its widest is ~12 km. The southern wall is 2.8 km high, and

the northern wall has a height of ~1.8 km (Schenk et al. 2018). We will show that this region is associated with enhanced abundance of water ice (Section 2.2) and ammonia (Section 2.3).

The main structural components in the western end of Virgil Fossae are shown in Figure 2.

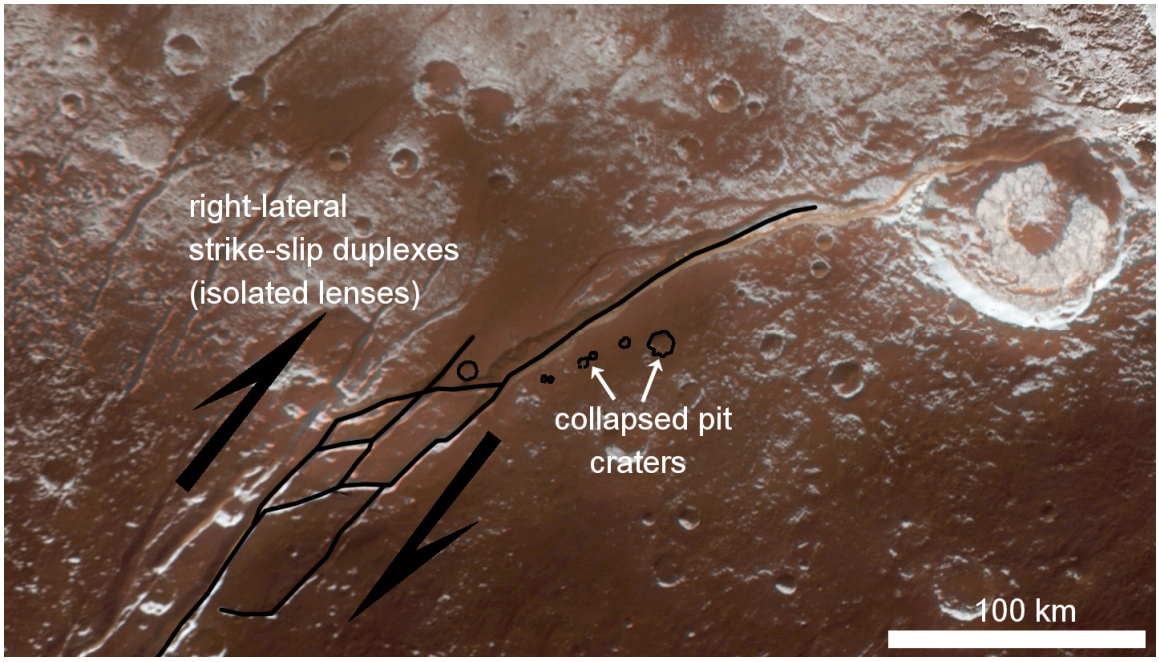

Figure 2. West of Elliot crater, components of the Virgil Fossae complex exhibit morphology consistent with strike-slip duplexes ("isolated lenses" are shown as black line segments).

Strike-slip duplexes seen in Figure 2 are most likely caused by a component of strike-slip motion (arrows) on the faults (Woodcock and Fisher 1986; Kim et al. 2004), which could arise from local crustal heterogeneities and thus local stress field anisotropies. A sub-parallel chain of sub-rounded, rimless depressions may be mantled impact craters, or pit craters caused by surface collapse into dilatational voids at depth (Wyrick et al. 2004; Runyon 2011). Thus the Virgil Fossae graben troughs are interpreted here to be caused by dilatational dip-slip normal faults with a right-lateral strike-slip component. Unresolved fractures likely make up complex fault damage zones (e.g., Kim et al. 2004) and would enhance subsurface hydraulic permeability of fluids in the manner of Caine et al. (1996).

In Figure 3, the elevation profile along a 250-km trace along the floor of the main trough of Virgil Fossae shows a vertical range of ~2 km, with higher points along the rim of Elliot crater.

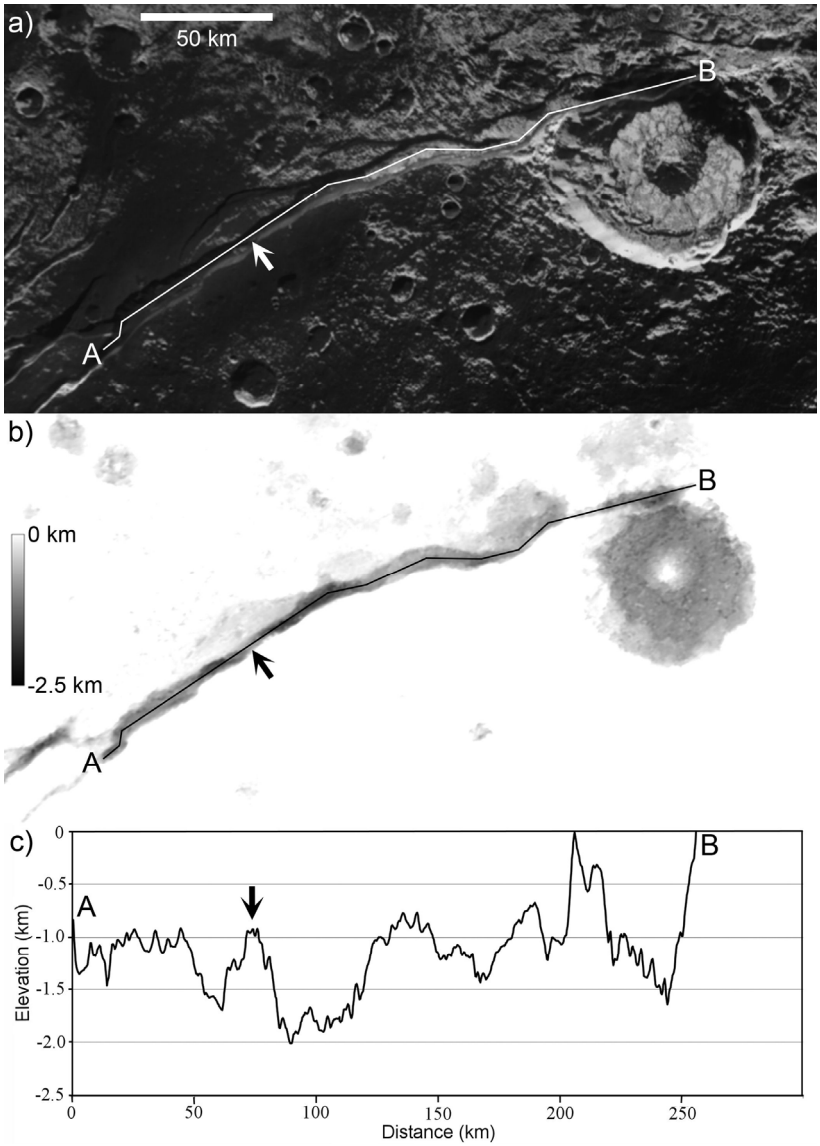

Figure 3. Virgil Fossae, Elliot crater, and a trace of the vertical relief along the floor of the main trough and across the crater's north rim. (a) a section of the base map (Schenk et al. 2018); (b) shaded elevation map; (c) relief along the trace through the trough. The arrow in each panel indicates the high point in the trough that is approximately coincident with the apparent center of effusion of the blanket of cryoclastics in the trough, on the rim, and beyond, and consisting of H_2O bearing the NH_3 spectral signature and the very red color specific to this region.

2.2 Detection of H_2O ice in Virgil Fossae and surroundings

LEISA spectra of Cthulhu are characterized by distinct H_2O absorption bands at 1.5 and 2.0 μm. The most prominent water ice exposures are found in the terrain surrounding Virgil Fossae, extending 100-200 km to the north and south (Figures 4a,b). The strong absorption in this region likely indicates higher concentration of water ice (although the strength may also arise from ice with larger grain size). The spectral characteristics of the H_2O bands, particularly at 1.65 μm, show that most or all of the ice is in the crystalline phase. The strong presence of crystalline H_2O ice is demonstrated in three independent analyses of the LEISA data (Protopapa et al. 2017; Schmitt et al. 2017; Cook et al. 2018).

The sunlight illumination of the Virgil Fossae region and the northern portion of Cthulhu are amenable to reliable spectral imaging, enabling the reliable extraction of the H_2O ice component of the signal. Extraction of the ammonia spectral signature described below that is critical to the subject of this paper is more difficult, and is described in detail in a separate paper by Dalle Ore, et al. (2019).

Figure 4a,b shows a section of the Pluto base map in enhanced color (Schenk et al. 2018) and the superposition of a map of the H_2O ice distribution (in blue) from Schmitt et al. (2017). The base map was constructed from high-resolution images with MVIC and that of the H_2O ice distribution from lower resolution LEISA spectral imaging.

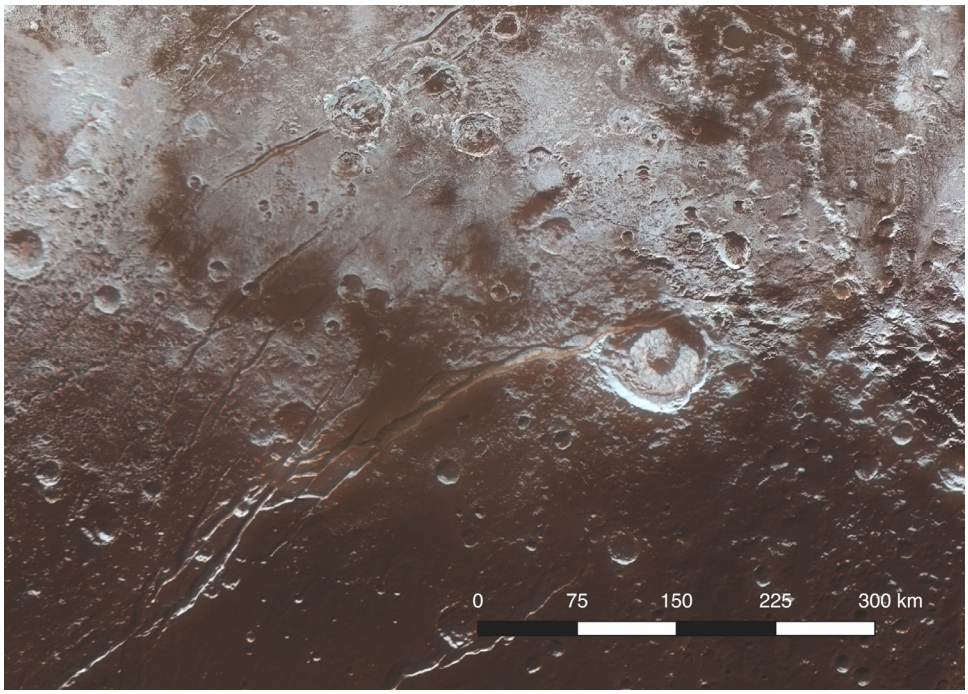

Figure 4a. The region of Virgil Fossae, Elliot crater and surroundings with enhanced coloration, excerpted from the Pluto base map (Schenk et al. 2018).

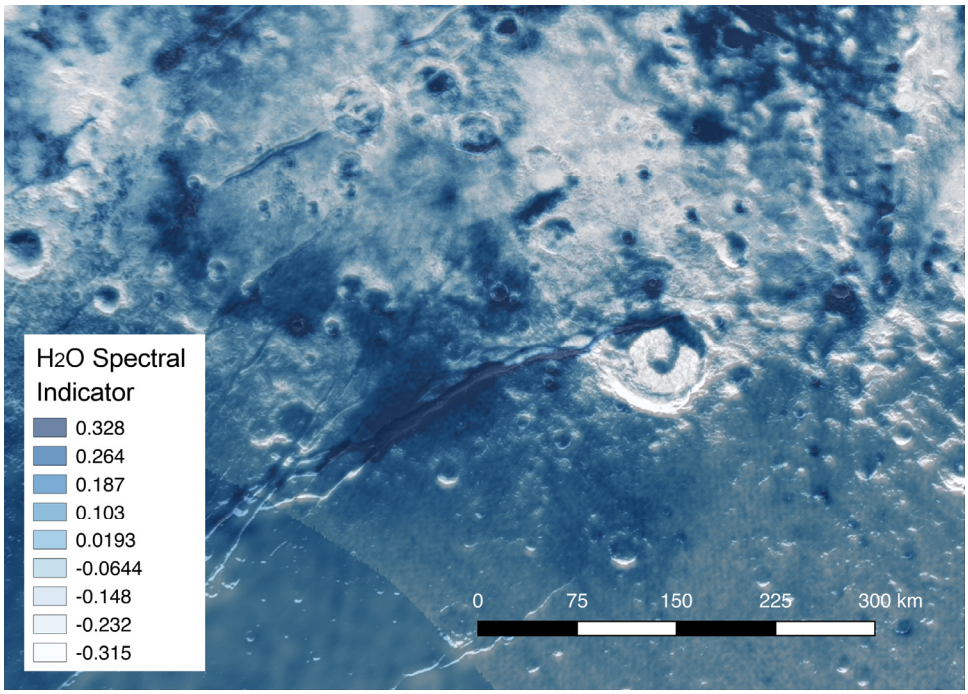

Figure 4b. The distribution of H_2O ice (blue) in Virgil Fossae and surroundings is shown by the superposition of the map of H_2O ice from Schmitt et al. (2017) on the base map (black and white monochrome.) The H_2O spectral indicator is the depth of the 2.0-μm H_2O band relative to the continuum around 1.38 μm, as defined in Schmitt et al. (2017); higher values (darker blue color) indicate stronger absorption in the major H_2O spectral bands measured in LEISA data.

Figure 5a is an enlargement of a section of Figure 4a, showing several examples of muted topography, interpreted here as mantling by H_2O ice covering preexisting craters and graben. The thickness of the putative mantling layer outside the trough appears to be less than ~100 m, which is approximately the limit of the stereo imagery in this region of the surface. The digital elevation map in this region does not have sufficient height resolution to demonstrate convincingly that features in the terrain are muted, and the lighting is such that photoclinometry using soft shadows is similarly inhibited. We instead interpret the visual appearance of various features in the region to suggest that a blanket of cryoclastics has been explosively ejected from one or more sources, most likely focused within Virgil Fossae along the south wall defining the graben. This issue is explored further in Section 5. The topography along the floor of the main trough of the fossa is irregular, ranging from ~400 to ~1400 m below the mean datum (the relatively flat terrain along the south rim of the trough).

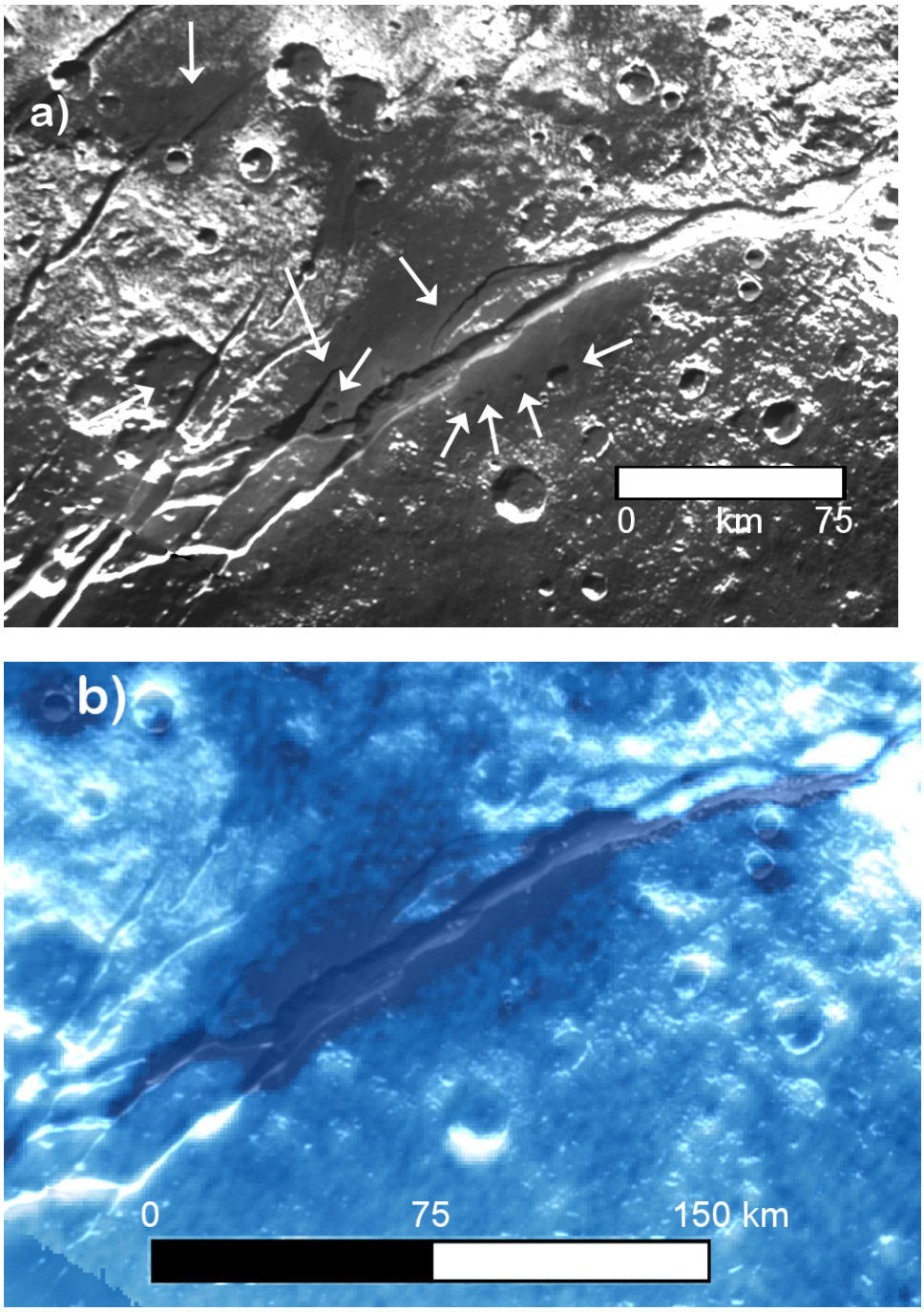

Figure 5. (a) Examples of muted topography interpreted to be mantled by H_2O ice in Virgil Fossae and surrounding terrain (white arrows). (b) Enlargement of a section of Fig. 4b, showing the high concentration of H_2O ice (darker blue) in and proximal to the main trough of the graben, and following the south wall.

Figure 6 shows the Pluto base map with an overlay of blue color in which the color intensity is proportional to the strength of the H_2O spectral absorption bands and is

codified in the H_2O spectral indicator inset from Schmitt et al. (2017). Colored lines against the background image denote three provinces around Virgil Fossae identified by their unique color, composition, and geomorphology. The areas outlined in white and yellow delineate regions where H_2O ice is most abundant based on LEISA data; weaker H_2O signatures (lighter blue color in the overlay) occur in this and adjacent parts of Pluto's surface. The area outlined in yellow denotes a region that is rich in H_2O and NH_3 found together in the spectral map. This combination of H_2O and NH_3 is more spatially extended than shown, and investigations in progress will delineate other parts of Pluto's surface where the two spectral signatures are found. The third area (outlined in red) is the region proximal to Virgil Fossae that includes the most mantled terrain where craters and topography of nearby, smaller fossae troughs are notably subdued.

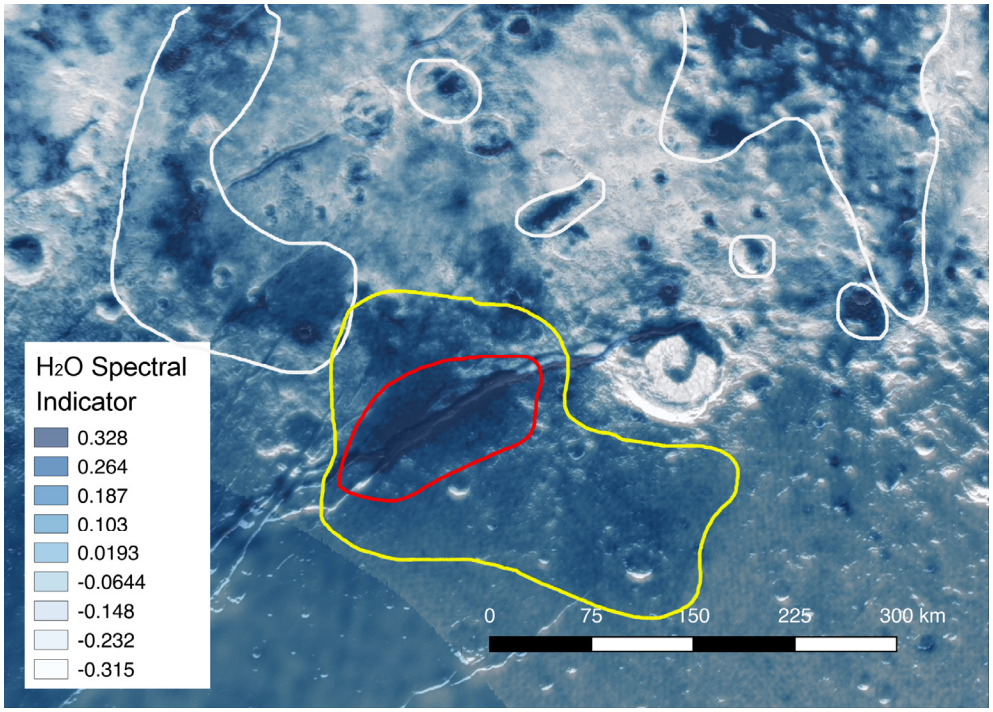

Figure 6. H_2O ice distribution (in the blue overlay on the base map) is shown in the Virgil Fossae area as described in the text. The red outline defines the region with the strongest H_2O spectral indicator, which is defined in Schmitt et al. (2017); see caption to Fig. 4b.

A striking feature within the main trough of Virgil Fossae and cutting across the northern rim of Elliot crater is the orange-colored material seen in Figure 1 and shown in the colorized highest resolution image available in Figure 4a. Comparison with Figures 4a and 4b shows that the colored material is spatially coincident with the distribution of H_2O ice in the fossa trough.

2.3 Detection of Ammonia in Virgil Fossae

In a statistical study of LEISA spectral images in the Virgil Fossae region, Dalle Ore et al. (2019) detected the signature of ammonia (NH_3) at 1.65 and 2.2 μm, which is expected to occur in the form of a hydrate of ammonia ($NH_3 \bullet nH_2O$) or an ammoniated salt. The two spectral bands are found in association with the H_2O ice absorption bands and are strongest where the H_2O bands are strongest, specifically in one section of the main component of the Virgil complex. Identification as a hydrate or a salt is ambiguous at the spectral resolution of the data. Figure 7 shows that outside the fossae, the NH_3 concentration becomes weaker but is still clearly present, as the H_2O ice spectral bands become weaker or are masked by the presence of CH_4 absorption bands. It follows that the observed spectral bands of NH_3 and H_2O parallel each other closely in relative strengths and spatial distribution.

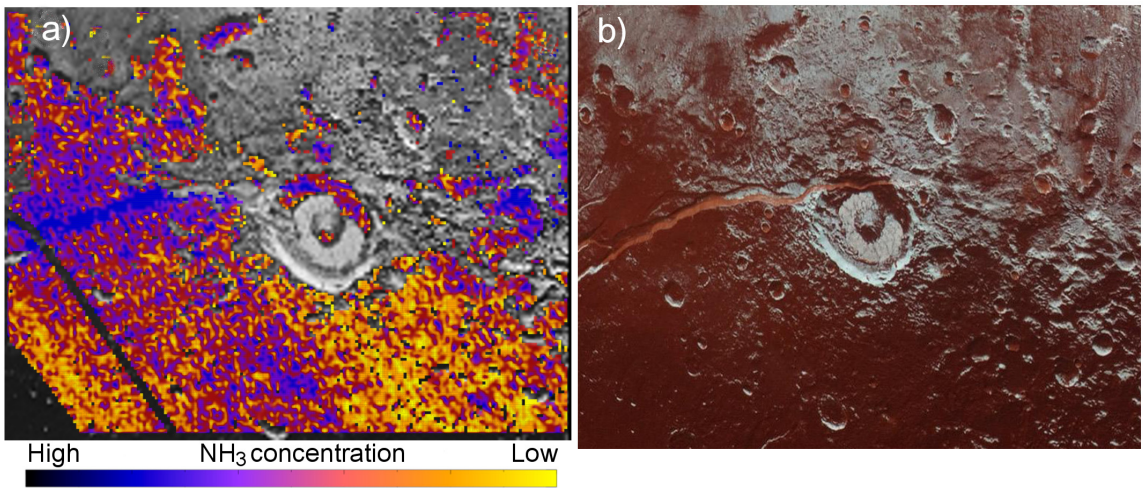

Figure 7. NH_3 map from Dalle Ore et al. (2019). a) Distribution of the ammonia spectral signature in the region of Virgil Fossae and Elliot crater. Blue represents the strongest absorption band, and yellow the weakest (but still detectable). Regions in gray do not show the NH_3 signature, but are seen in other data to have strong CH_4 absorption. b) The same geographic region, from the composite MVIC image pmap_cyl_KH201.

If the ammonia signature in the H_2O ice in the exposure found at Virgil Fossae represents an ammonia hydrate, there is an unresolved ambiguity in the hydration state. The ambiguity arises from the similarity in the reflectance spectra of pure NH_3 ice and a frozen hydrate, which could be $NH_3 \bullet 2H_2O$, $NH_3 \bullet H_2O$, or $2NH_3 \bullet H_2O$. Hydrates naturally form as liquid H_2O reaches the freezing point and nanocrystals form in the presence of NH_3 (Uras and Devlin 2000), and also as an ice composed of H_2O and NH_3 is warmed (Moore et al. 2007). Similarly, hydrates form as NH_3 diffuses through H_2O ice when the concentration of NH_3 exceeds the solubility limit. The diffusivity of NH_3 hydrate in H_2O ice is much greater than that for free molecules of many species. However,when the diffusion coefficient for the hydrate is extrapolated from the temperatures at which it is measured in the laboratory (140K) to Pluto's surface temperature (~45K), the diffusivity is vanishingly small (Livingston et al. 2002). We note that Livingston et al. caution against a simple extrapolation of their measured values of D to much lower temperatures, but it is reasonable to expect that at a temperature 100 K lower than in their experiments the value of D will be much lower than the ~10^{-10} cm^2 s^{-1} that they measured. It may be

the case that at slightly warmer temperatures in the ice column below the uppermost surface, NH_3 hydrate diffuses more rapidly upward along a negative concentration gradient, and that it eventually arrives at the visible surface where we detect it spectroscopically (Dalle Ore et al. 2019). The diffusion of NH_3 hydrate through porous ice is much faster than in dense ice, and while we might speculate that ice exposed at Pluto's surface at T~40K for very long times could be quite porous, there is no supporting direct evidence.

Another possible source of the ammonia signature at Virgil Fossae is an ammoniated salt. Some of these salts show a band near 2.2 μm characteristic of the NH_4^+ ion (Moore et al. 2007); it lies at a slightly shorter wavelength than the NH_3 band. In reflectance spectra obtained at RELAB (Brown University), ammonium salts (e.g., $(NH_4)_2CO_3$, $(NH_4)_3PO_4$, $(NH_4)_2SO_4$, NH_4Cl) show fairly broad absorption bands with the absorption peaks in the range 2.15-2.17 μm (Berg et al. 2016). (DeSanctis et al. (2015, 2016) use ammoniated salts NH_4Cl and $(NH_4)_2CO_3$ as components of a fit to the spectrum of bright regions on Ceres obtained with the Dawn spacecraft over a broad wavelength range that included 2.2 μm. In addition, Cook et al. (2018) have shown that NH_4Cl is a good spectral match to the 2.2-μm absorption band in the spectrum of Pluto's satellite Nix. Ammoniated salts appear to be viable candidates for surface materials that exhibit an absorption band near 2.2 μm. The available spectral data for Pluto, Nix, and the other satellites do not extend to the longer wavelengths ($\lambda > 2.5$ μm) where additional diagnostic spectral bands of ammoniated species occur.

In the absence of reliable complex refractive indices for NH_3 hydrates and ammoniated salts, and in view of the intrinsic limitations of the spectroscopic data for the ammonia signature, we are presently unable to distinguish between these two plausible alternatives through modeling techniques. A simple comparison of the band shapes and positions does not resolve the ambiguity.

While the state and phase of NH_3 in H_2O at the visible surface of Pluto are important to the practical matter of its persistence in the space environment and its detection by remote sensing, ammonia is a critical component that affects the evolution of an interior ice layer or fluid reservoir. Models calculated for Triton, but relevant to Pluto, describe the thickening of an ice shell and the concentration of NH_3 in the uppermost few kilometers (Hammond et al. 2018). As the concentration of NH_3 increases, the freezing temperature is depressed, while the increased buoyancy of the fluid exerts an upward pressure on the crust that may enhance its ability to emerge onto the surface.

3. Photon, solar wind particles, and cosmic ray destruction of NH_3

Understanding the longevity of the NH_3 spectral signature in the Virgil Fossae region is critical to an estimate of the age of its emplacement. We therefore consider three mechanisms in Pluto's natural environment that lead to the destruction of NH_3 in H_2O, although substantial uncertainties in the rate of destruction remain because of the unknown hydration state of the NH_3 or the anion corresponding to the NH_4^+ cation if salts are present.

3.1 Destruction by Lyman-α radiation

Ammonia on Pluto's surface, in whatever form it occurs, can be destroyed by solar or interplanetary Ly-α photons. The Ly-α flux is limited by the opacity of the (current) atmosphere resulting from absorption by gaseous CH_4. While the atmosphere may have been significantly more dense in past epochs (see Stern et al. 2017, Bertrand et al. 2019), there is no direct evidence that it was ever completely absent. However, in some of Bertrand's simulations over a 30-My time period, changes in the CH_4 mixing ratio result in changes in the atmospheric transparency to Ly-α radiation, which can vary from 0.01% to 10%. The variability in transparency tracks the changing patterns of condensation and evaporation of CH_4 on the surface, which in turn depend on the albedo of the CH_4 deposits. For example, when N_2 ice covers and thereby traps Pluto's equatorial CH_4 deposits, the CH_4 mixing ratio in the atmosphere is less than 0.01% over an entire year, and a significant flux of Ly-α reaches the surface, where it can readily photolyze NH_3 and exposed hydrocarbons.

At Pluto's heliocentric distance of 40 AU, the Ly-α radiation directly from the Sun is ~$3x10^8$ photons/cm^2/s. The interplanetary medium beyond Pluto is also a source of Ly-α (Gladstone et al. 2018), measured with the New Horizons spacecraft, with a flux of ~$4.3x10^7$ photons/cm^2/s, or ~15 percent of the direct solar flux. Thus Pluto and its satellites are bathed in Ly-α at all times. Free ammonia or NH_3 frozen in H_2O ice is readily dissociated by Ly-α (10.2 eV/photon), while ultraviolet radiation at other wavelengths, as measured at Pluto by Steffl et al. (2019), is efficient in photolytic processing of CH_4 and other hydrocarbons. The penetration depth of UV photons into NH_3 (or other) ice is only a few micrometers (Bennett et al. 2013 table 4). Gardening of the surfaces of these bodies at the level of millimeters could expose fresh layers of NH_3-H_2O, even as the uppermost few nm are depleted. At Pluto (and Charon) the gardening rate is unknown because the impact rate of small impactors and dust is not well known. On the basis of lunar gardening models and in consideration of particles originating in the Kuiper Belt and from the four small satellites of Pluto, Grundy et al. (2016) estimated gardening on Charon's surface to centimeter depths in ~10^7 y. If the shallow size distribution found for ~300-m to 1-km impactors extends to even smaller impactors (Singer et al. 2019), then this would lead to reduced gardening rates.

We are unaware of experiments to measure the dissociation of ammoniated salts by UV photons.

For NH_3 in ice, the *rate* of net destruction likely depends on the nature of the ice in which it is frozen. For example, in a pure NH_3 ice, irradiation largely results in the dissociation of H atoms from the parent NH_3 to form NH_2, which can combine to form N_2H_4 (diimide) (Loeffler and Baragiola 2010a). The H atoms can combine with NH_3 to form NH_4^+ (Moore et al. 2007) and can combine with each other to form H_2 (Loeffler and Baragiola 2010b), which can ultimately be lost from the ice. However, many H atoms will simply recombine with N to reform NH_3. In this case, the chemical sink of ammonia into other molecular species is relatively simple, and while ammonia is being destroyed it is also

being re-created. Consequently, the fading of spectral bands of NH_3 will be slower than suggested by the direct NH_3 destruction rate.

The presence of carbon-carrying species in the ice can change the NH_3 destruction process considerably. In addition to making simple O,C,N-containing species like OCN^- (Grim and Greenberg 1987, Demyk et al. 1998, Bernstein et al. 2000, Pilling et al. 2010), the destruction of NH_3 in C-bearing ices can lead to the incorporation of the ammonia's N atoms into a host of complex organic species (Allamandola et al. 1988). For example, Bernstein et al. (1995) showed that the UV irradiation of H_2O:CH_3OH:CO:NH_3 ices results in the incorporation of approximately half of the N in NH_3 into complex organic residues after exposures of only ~1 x 10^{20} photons cm^{-2}. The solar Lyman-α flux at Pluto averaged over its orbit, plus the interplanetary medium (with no extinction) is (~1.2 x 10^8 photons cm^{-2} s^{-1}) (Bertrand et al. 2019, eq. 2). At times of 10% transparency of the atmosphere (moderately strong CH_4 absorption), the resulting flux at the surface is ~1.2 x 10^7 photons cm^{-2} s^{-1}. With these parameters, the dose of ~10^{20} photons cm^{-2} at the surface corresponds to ~3 x 10^5 years. When the atmospheric transparency is 0.01%, the timescale for the reactions described above is ~ 3 x 10^8 y.

3.2 Destruction by solar wind charged particles

The plasma (e^-, H^+, He^{2+}) ejected by the Sun interacts with Pluto in a manner different from the interactions with other planets and satellites (McComas et al. 2016), and while the planet induces a bow shock in the solar wind ~4.5 R_p (~5300 km) upstream, the flow picks up CH_4 ions from the thin atmosphere and carries them a great distance downstream. These energetic heavy ions impact the surface of Charon, and are likely to induce chemical changes in the satellite's surface ices (Grundy et al. 2016b). Some energetic particles penetrate Pluto's atmosphere and impact the surface, also inducing chemical changes. One expected effect is to dissociate NH_3, adding to other effects that limit the lifetime of these molecules on the visible surface.

Secondary electrons produced by various MeV radiations (H^+, He^{2+}, e^-, X-rays, γ-rays) account for most of the interactions, and are independent of the original particle from which they originated (Hudson et al. 2008). The penetration depths for electrons and protons in ice are shallow, ranging from several nanometers to a few tens of micrometers for particles with energy <~ 1 MeV, and a few hundred micrometers to >1 mm for energies up to ~10 MeV (Bennett et al. 2013, Table 4). The depth in the ice to which we probe with near-infrared spectroscopy, as used to detect the NH_3 signature on Pluto, is a few micrometers, depending on the characteristics of the ice surface (granular or glazed). Thus the chemical alteration effects of the solar wind affect the optical signature detected by remote sensing.

Loeffler et al. (2010a,b) and other work have shown that the ammonia spectroscopic signature is readily destroyed by 100 keV protons in a NH_3-H_2O ice at temperatures >120K, but destruction is slow at lower temperature. In the case of the ammonia signature on Charon, presumed to be that of ammonia hydrates, Loeffler et al. (2010a,b) estimate that about 40% or more of the original ammonia has been removed from the

optical surface over the age of the Solar System by impinging protons. We have addressed the issue of NH_3 diffusion through H_2O ice elsewhere in this paper, but we note that Holler et al. (2017) have suggested that diffusion of ammonia through Charon's surface ice might explain the persistence of the spectral signature over time. Alternatively, if the original concentration of NH_3 on Charon was high, the loss estimated by Loeffler et al. (2010a,b) may be consistent with observations in the current epoch.

3.3 Destruction by galactic cosmic rays (GCR)

Charged particles in GCRs interact with Pluto's atmosphere and penetrate the solid surface where they ionize the subsurface environment. Energetic particles can undergo hadronic interactions and produce secondary particles, which in turn undergo further interactions, depending on their energy, and ionize the path they traverse. In order to model these interactions, we used the Geant4 particle interaction model (Agostinelli et al. 2003; Dartnell et al. 2007; Atri 2016). The code tracks individual particles and models all known particle interactions, and has been experimentally calibrated. Two layers were constructed for the computations, (1) the top layer, where charged particles were incident, which represented the atmosphere, and (2) the bottom layer, which represented the solid surface.

For these calculations, Pluto's atmospheric composition was set to 95% N_2, 4% CH_4, and 1% CO and the arbitrarily deep solid surface was set to a 30/70 mixture of NH_3 and H_2O ice. The atmospheric composition is generally consistent with the current atmosphere and the NH_3:H_2O mixture is an estimate of an unknown quantity. Since Pluto's atmosphere has shown indications of variability, two types of atmospheric models were considered -- with 1 and 100 microbar atmospheric pressures, keeping the same chemical composition. We assumed that Pluto has no magnetic field and the GCR spectrum was incident on the top of the atmosphere with 10^9 primary particles. The output was the averaged energy deposition profile below Pluto's surface as a function of depth. Since our main objective was to compute NH_3 dissociation, the energy deposition cutoff was set to 10.5 eV and particles with lower energies were discarded. The dissociation energy of the N-H bond in NH_3 is 10.2 eV. Simulations showed that the output from 1 to 100 microbar atmospheres were indistinguishable within numerical errors. This was expected since GCR particles can easily penetrate such a thin atmosphere and energy deposition in the solid surface is mainly done by higher energy particles. The output shows the energy deposition rate as a function of depth in eV/g/s (Figure 8). The same calculation was made for a pure H_2O solid surface, but the difference between that model and the 30/70 NH_3 - H_2O mix model is only about 3%, owing to the small difference in the neutron count between pure H_2O and the mixture. For the present discussion, we ignore that small difference.

Figure 8 shows that the energy from GCR and the secondary products in a layer of H_2O-NH_3 on Pluto's surface is mostly absorbed in the uppermost one meter. Using the value 10^7 eV/g/s, which is the calculated energy deposited in the first meter of the surface, we calculate the time required to destroy all of the NH_3 molecules. The molecular mass of

NH_3 is 17.03 g/mole, corresponding to 3.5 x 10^{22} molecules per gram mass. Dividing the number of molecules by the destruction rate gives ~1.1 x 10^9 years to break at least one N-H bond in all the NH_3 in the one-meter surface layer. Ammonia can be detected spectroscopically at the level of ~3% in H_2O (Dalle Ore et al. 2019), so the time to destroy 97% of the NH_3 in the upper meter of the surface is ~10^9 y. However, as noted above, in the unlikely absence of other atoms or radicals, the N and H atoms might combine to remake NH_3 in a relatively self-sustaining process. If the supply of the NH_3 to the surface is static, this time gives an upper limit to the age of the material observed in the Virgil Fossae area. Thus, with the diffusion rate near zero, the NH_3 we detect can be as old as ~10^9 , or even older if NH_3 is remade in the upper few meters of the surface.

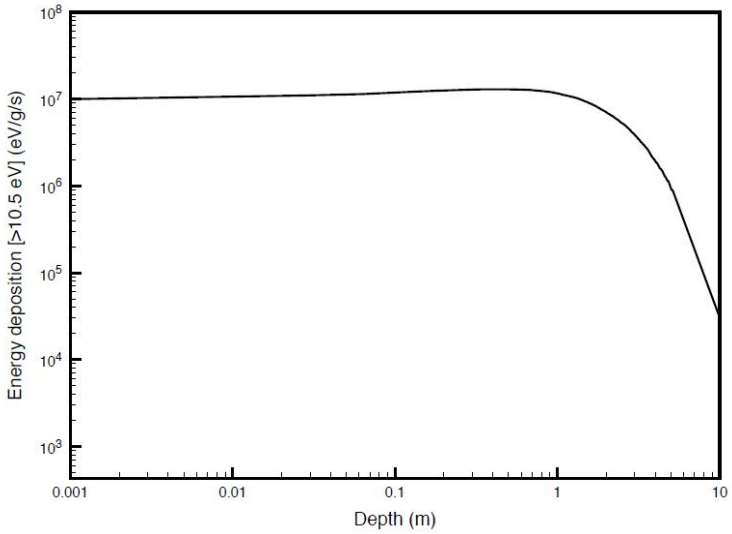

Figure 8. Energy deposition with depth of galactic cosmic rays with energy >10.5 eV in a surface ice layer of NH_3+H_2O mixed 30% NH_3 and 70% H_2O in Pluto conditions.

For all three mechanisms considered here, the loss of NH_3 spectral features can be accelerated in ices that contain other molecular species since these will allow the molecular fragments of NH_3 to form new species that are less likely to be converted back into NH_3. For example, irradiation of NH_3 in the presence of oxygen-bearing species like H_2O can lead to the formation of some simple oxides like NO and N_2O (Loeffler et al. 2010a,b, Pilling et al. 2010).

The uncertainty in the rate of hydrate destruction by ultraviolet radiation and energetic atomic particles, as well as the possible refreshing of the ammonia by diffusion from below, leave as an open question the lifetime of the ammonia spectral signature observed in the LEISA data for the Virgil Fossae region. The persistence of the spectral signature on Charon and two small satellites support the view that a combination of destruction and recharging of the ammonia content of the optical layer of an ancient H_2O-rich surface serve to retain the observed spectral signature on Gy timescales.

The time scales of the three processes considered here for the destruction of NH_3 in H_2O range from an upper limit of ~10^9 years by GCR to a much shorter timescale of ~10^5

years when the atmosphere is ~10% transparent to Ly-α radiation. Although unlikely, as outlined above, refreshment of the ammonia content of the upper surface probed by optical spectroscopy by diffusion through the H_2O could potentially prolong its presence for long periods.

The H_2O-rich surface in the Virgil Fossae region is clearly younger than the age of the planet, but the use of the observed ammonia spectral characteristics and the vagaries noted here leave the actual timescale of emplacement and modification incompletely resolved.

4. Nature of the red-colored component

A range of colors from pale yellow to orange, red, and dark brown is seen over most of the hemisphere of Pluto imaged at high resolution by New Horizons (the encounter hemisphere) (e.g., Olkin et al. 2017). This color is generally attributed to the presence of a relatively refractory non-ice component that may consist of a complex mixture of organic molecules and broadly defined as tholins (Grundy et al. 2018, Cruikshank et al. 2005, 2019).

The red-colored material running nearly the full length of the main trough and some components of the graben of Virgil Fossae is also seen in several nearby craters, on the surrounding terrain (particularly to the southwest), and in limited portions of the main trough of Beatrice Fossa. Olkin et al. (2017) note that this color is different from the colors found elsewhere on the encounter hemisphere of Pluto and is different from the color diffusely distributed on Charon's north polar region. The geographic distribution of this material eliminates its formation and deposition from an atmospheric source and instead supports the contention that it emerged on the surface in a fluidized state from some unknown depth in Pluto's interior. The presence of the material in several nearby craters suggests that they are also associated with conduits to the subsurface source, perhaps as a consequence of fractures of the local crust at the time of the impacts forming the craters. The areal distribution of craters so affected may help define the horizontal extent of the putative reservoir. The depth to which such fracturing extends may indicate the thickness of the crust above the reservoir.

We posit that the tholin or the molecular material that led to its formation was present in the fluid comprising the reservoir, and suggest that its organic contents represent processed material from the feedstock from which Pluto aggregated in the solar nebula. Pluto's bulk density is 1.854 ± 0.006 g/cm^3 (Nimmo et al. 2017), and in the model by McKinnon et al. (2017) the composition is represented by water ice and partially hydrated rock of solar composition in the ratio rock/(rock+ice) = 0.655 ± 0.005. Judging from the material preserved in comets and carbonaceous meteorites, the rocky material of solar composition also included a significant organic component consisting of both soluble and insoluble organic compounds (e.g., Pizzarello et al. 2006, Wooden et al. 2017). It is generally acknowledged that reactions leading to organic molecules occurred both on cold interstellar dust grains and, after accretion in the protosolar nebula, through aqueous reactions in the meteorite parent bodies (Pizzarello et al. 2006), while recent

isotopic analysis supports the view that the some of the chemistry creating the complex molecular inventory of comets and meteorites occurred in the protosolar nebula (Tartèse et al. 2018), possibly from processed carbon-rich precursors.

Additional processing of organic material incorporated during the formation of Pluto may have taken the path described by Kebukawa et al. (2017). They demonstrate in the laboratory that aqueous processing of a solution of simple organic molecules (formaldehyde, glycolaldehyde, and ammonia, all of which are found in comets and interstellar gas and dust) in the presence of complex, macromolecular solids similar to the insoluble organic matter in carbonaceous meteorites are amino acid precursors. These reactions proceed in liquid water in the absence of ultraviolet photons or charged particles, as would be the case in a planetary interior. Shock (1993) has shown how dehydration reactions in warm hydrothermal systems promote many reactions in organic chemicals, including peptide formation from amino acids.

Neveu et al. (2017) have modeled the interactions of liquid water and rocky material of chondritic composition and with a fluid consisting of C, N, and S in proportions derived from observations of comets. Both the chondritic rocky material and the comet fluid contained organic material patterned after the insoluble organic matter (IOM) in carbonaceous meteorites. Among the modeling results related to ammonia, Neveu et al. (2017) found consistency with the detection of ammoniated phyllosilicates, and NH_4CO_3 and NH_4Cl on Ceres. They further find that NH_3 in water in the interiors of icy bodies does not react with the initial organic matter, but can be oxidized to N_2 and lost to the fluid either in this molecular form or as NH_3 gas. In the protonated form NH_4^+, it is removed from the fluid through the formation of minerals and salts. In cold fluid-chondritic systems, N is predominantly found in ammoniated minerals.

In a Pluto subsurface hydrothermal system that we propose here, the occurrence of a combination of ammoniated minerals and salts, as well as a complement of complex macromolecular organics appears to be well within the parameters of formation and evolution of the red material explored by the laboratory experiments and models cited here and as described in detail by Cruikshank et al. (2019).

5. Cryovolcanism at Virgil Fossae

5.1 The Planet-scale Geophysical Setting

A quantitative geophysical understanding of cryovolcanism on icy worlds is challenging. The primary obstacle for the ascent and eruption of a fluid is buoyancy; liquid water is denser than water ice. For liquid water to ascend to the surface it must be over-pressurized by some mechanism. The simplest such mechanism is the freezing of a subsurface ocean or a cryomagma chamber. As the water within the ocean or chamber freezes, it expands, generating an overpressure that can result in rupture of the chamber and the ice shell, resulting in the eruption of the liquid water (e.g., Fagents 2003, Manga & Wang 2007, Neveu et al. 2015, Lesage et al. 2018).

A planet-scale geophysical characteristic of Pluto may have facilitated cryovolcanism at Virgil Fossa and perhaps other structures nearby. Pluto likely underwent at least one episode of true polar wander (reorientation of the body with respect to the rotation and tidal axes) due to the formation of Sputnik Planitia, and the loading of that region with the large, thick glacier of nitrogen ice (Nimmo et al. 2016, Keane et al. 2016). The combination of global expansion (driven by the freezing of a putative subsurface ocean), true polar wander, and loading generated substantial tectonic stresses in Pluto's lithosphere. Keane et al. (2016) calculated these stresses using Love number theory and used these stresses to predict the orientation of Pluto's faults. The predicted geometry very closely matched the observed geometry of Pluto's faults. However, Keane et al. did not investigate the actual magnitude of these stresses. Reanalysis of those results reveal that the actual magnitude of the extensional stresses is maximized in an annulus around Sputnik Planitia that includes Virgil Fossae and the other putative cryovolcanoes, Wright Mons and Piccard Mons (Figure 9). This new result is not strongly sensitive to the presumed interior structure of Pluto or the true polar wander scenario.

Enhanced extensional stress at Virgil Fossae may facilitate cryovolcanism. The extensional stress effectively reduces the overburden pressure, thus reducing the threshold for a subsurface fluid chamber to rupture via tectonic pressurization (Hanna and Phillips 2006; Hammond et al. 2016). Detailed modeling of the generation and ascent of the fluid is beyond the scope of the work presented here.

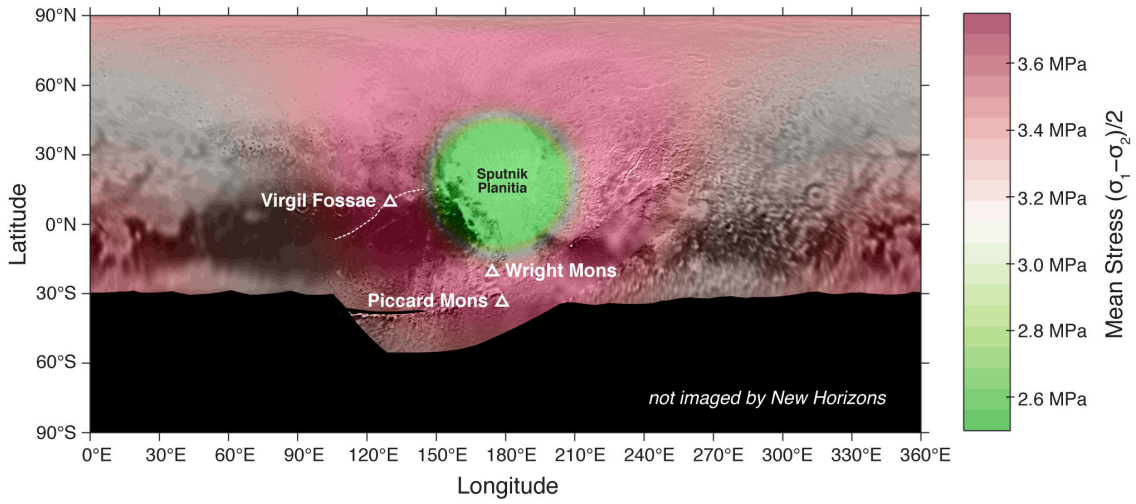

Figure 9. Mean stress at the surface of Pluto predicted by the true polar wander, global expansion, and surface loading models of Keane et al. (2016) in color, superimposed on the Pluto base-map. In this model Sputnik Planitia is mass-loaded with a nitrogen ice glacier with an uncompensated exponential thickness profile: $h = h_0 \exp(-\varphi/\varphi_0)$, where h is the thickness and φ is the angular distance from the center of Sputnik Planitia. We assume h_0=1 km and φ_0 = 20°. The combination of stresses from the loading of Sputnik Planitia, the resulting true polar wander, and global expansion due to the freezing of a subsurface ocean, produce these tectonic stresses. The mean stress is the average of the two principal stresses, σ_1 and σ_2, and is positive for extensional stresses. This predicted

pattern of extensional stress is not strongly sensitive to these parameters or the overall load profile. These extensional stresses maximize in an annulus around Sputnik Planitia that includes Virgil Fossae and the other putative cryovolcanic features, Wright Mons and Piccard Mons (e.g., Moore et al. 2016, Singer et al. 2016b). Extensional stress reduces the overburden pressure and likely increases the ease by which a fluid can rupture Pluto's crust and ascend to the surface.

5.2 Emplacement of a Fluid by Flow

The physics of the emergence onto Pluto's surface from a subsurface reservoir of a fluid mixture of water, ammonia in some form, and dissolved or particulate organic material, is complex, and depends on many factors that are unknown. Fluid temperature and viscosity, column geometry, ejection volume and pressure, and the temperature of the surface are among the parameters that must be modeled in order to estimate the extent of a flow of cryolava (Umurhan et al. 2019).

In the liquid phase, the addition of NH_3 to H_2O reduces the freezing temperature of the mixture by as much as ~100 C below the normal freezing temperature of pure H_2O. The consequences of the lower freezing temperature are that a reservoir of this mixture in Pluto's mantle can remain liquid for much longer as internal heat from the decay of radioactive elements in the rocky component of the planet dwindles over time (see Nimmo et al. 2016). In addition, as we note below, NH_3 in H_2O increases the viscosity of the mixture (Kargel et al. 1991), but with increasing NH_3 concentration, the density of the fluid decreases, making it more buoyant (Hammond et al. 2018). The ensuing pressure in the reservoir may be a factor that affects the ejection of a fluid from vents on the surface, either as a flow or as a fountain (or both), as discussed in more detail in Umurhan et al. (2019). The chemical consequences of a molecular mix of NH_3 and H_2O are considered from the point of view of the synthesis of complex organic molecules by Cruikshank et al. (2019), as already discussed.

In the main trough of the Virgil Fossae complex, the red-colored material traces the emplacement of a fluid that appears to have debouched along the fault that defines the south wall and extends for more than 200 km along the trough. The altitude profile along the floor of the trough over the extent of the colored deposit shows a vertical range of more than 2 km, with the high points coincident with the north rim of Elliot crater (Figure 5). This profile is clearly inconsistent with flow along the trough, and is more easily explained as effusion along the fault. The flow of a H_2O-NH_3 fluid on Pluto is limited by several factors, particularly the rapid freezing of the fluid as it emerges into the cold vacuum of the planet's surface environment.

The calculations by Umurhan et al. (2019) consider several factors governing the freezing of a creeping H_2O-NH_3 cryolava. The scenario envisioned is a cylindrically symmetric flow of cryofluid pouring over a cold, highly conductive bedrock surface. The flow is considered choked off after that time at which the thickness of the head of the creeping flow equals the total amount of vertical freezing that would have occurred over that same period of time. It is also found that freezing is dominated by thermal conduction into the

cold surface bedrock and that freezing driven by radiative losses into the vacuum above occurs much more slowly. Finally, we note the apparently counter-intuitive trend that, for all other parameters held equal, for larger viscosities a flow will extend much further before freezing than for smaller viscosities. This is explained by noting that a lower viscosity flow will result in the head of the flow extending out farther much faster than the case of a more viscous flow. This, in turn, means that the lower viscosity flow will thin out sooner and thereby freeze more readily as it takes much less time to freeze a thin layer than a thick one.

Figure 10 shows model calculations of the distance that a slurry of ammoniated water can flow on Pluto's surface in terms of flow injection rate and viscosity (Umurhan et al. 2019). These models suggest that under some circumstances the fluid could flow for a few kilometers from the source before freezing in place. In this context we note that in several places along the trough there are near-perpendicular extensions of the colored material that extend 1-3 km from the main trough and may represent break-outs of the fluid before it froze (Figure 11). Alternatively, the irregularities along the margin of the deposit may simply indicate rough terrain at a scale below the resolution limit of the image.

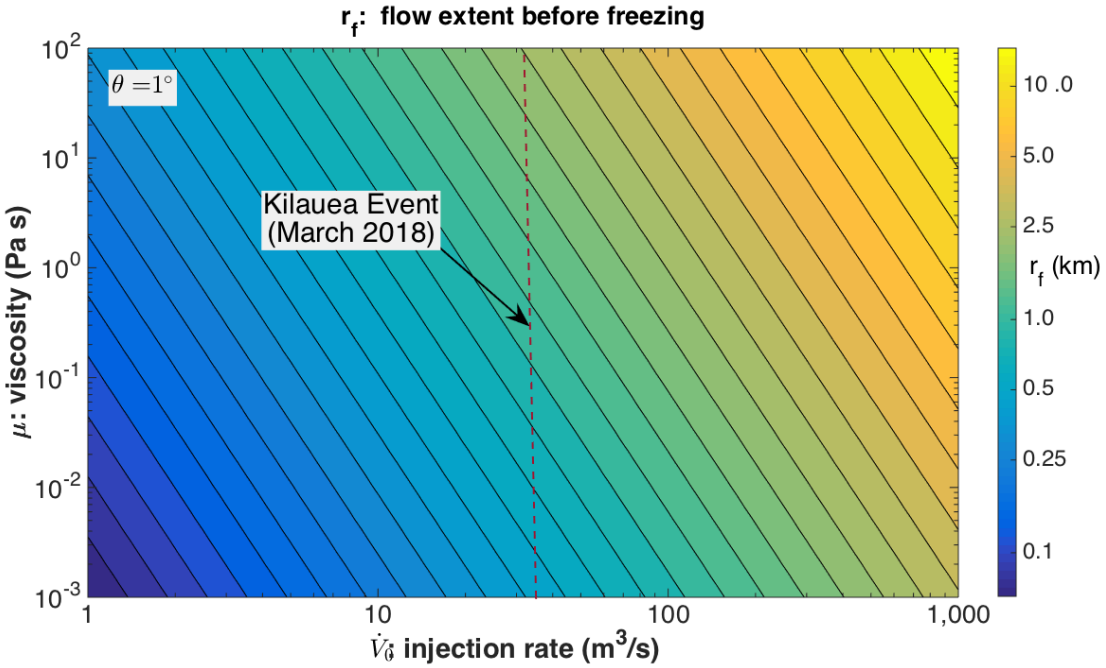

Figure 10. Contour plot of extent, r_f, of emergent NH_3 - H_2O slurry flow before freeze, based on calculations by Umurhan et al. (2019). Plot is shown as a function of flow injection rate versus viscosity, μ, of slurry, for a slope (θ) = 1°. The viscosity range follows values indicated by laboratory investigations of Kargel et al. (1991). A range of injection rates is shown, with the eruption at Kilauea Volcano (March 2018) indicated. The flow is assumed to be emplaced at a temperature T=200 K. Owing to the very weak dependence of r_f on the viscosity, the flow extent falls into the range of 0.1-10 km for most reasonable values of the flow quantities. The dependence on the initial slope of the landscape upon which the cryolava flows is also relatively weak. From Umurhan et al. (2019).

An approximate terrestrial analog of features of this kind is found on volcanic fissures that give rise to curtain-type eruptions in Hawaii and other shield volcanoes. Curtain eruptions usually occur in the earliest phases of an eruptive episode as a new fissure is forced open, and then subside as the pressure is relieved, but often with voluminous and long-lasting lava flows extending outward from the fissure.

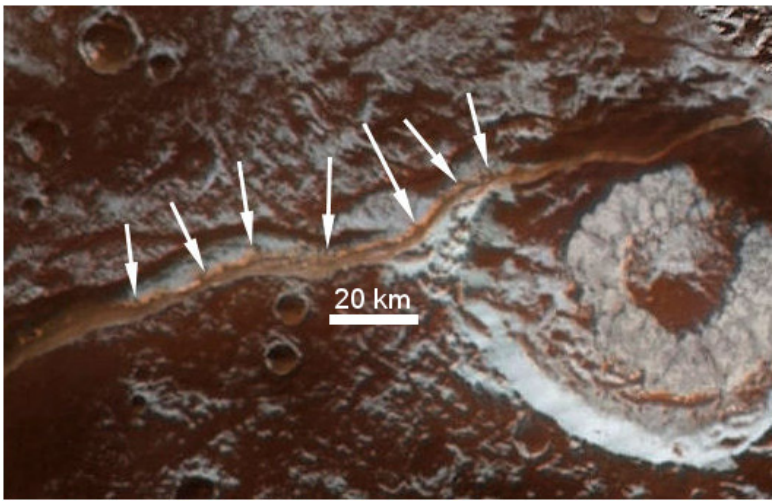

Figure 11 The deposit of red material along the south wall of the main trough of Virgil Fossae and up the northwest rim of Elliot crater extends over a range of elevation >2 km, and may represent an effusion of fluid along a fault. Arrows show possible break-outs from the main deposit.

5.3 Ballistic Emplacement of Ammoniated Water

Active ejection of materials from planetary surfaces has been observed directly, beginning with the discovery of volcanic plumes emanating from several sources on Io (Smith et al. 1979). The Io plumes consist of gas and silicate rock fragments, leaving dark surface deposits of high temperature that are consistent with mafic to ultramafic silicates. Elemental sulfur in a variety of its colored polymorphs, as well as deposits of frozen SO_2, are also found in the vicinity of several plumes (Williams & Howell 2007). Plumes have also been detected emanating from the south polar region of Enceladus by the Cassini mission. They consist of gas, H_2O, and complex organic molecular material (Hansen et al. 2011; Postberg et al. 2018), as well as salts and SiO_2 (Postberg et al. 2011; Hsu et al. 2015). Tian et al. (2007) estimate a plume ejection velocity in the range 300-500 m/s, which exceeds Enceladus' escape velocity (V_e = 239 m/s) resulting in the formation of the E-ring of Saturn (Hansen et al. 2011; Southworth et al. 2015). Europa may exhibit intermittent water vapor plumes that may also contain dust (Roth et al. 2014). The plume velocity at the vents on Europa is roughly estimated as 700 m/s by Roth et al. (2014) and in the range 300-500 m/s by Sparks et al. (2017), in either case below the moon's V_e of 2025 m/s. We note that Ruesch et al. (2016) have made a case for

cryovolcanism on Ceres carrying material initially rich in H_2O and depositing salts that include ammoniated species.

The ejection velocity of a plume originating inside the main trough of Virgil Fossa can be estimated from the distance that the effluent appears to have traveled on ballistic trajectories. In the simplest case, ignoring Pluto's thin atmosphere, the ballistic equation gives the horizontal range R versus the angle of ejection as

$$R = v^2 \sin(2\omega)/g,$$

where v is the velocity at the source vent, ω is the angle from the normal, and g is the acceleration due to gravity (0.62 m/s). Taking the maximum distance of the deposit from the source as R ~ 200 km from its appearance in Figure 5, v ~350 m/s for an ejection angle of 45º. If the angle of ejection is 10º to the vertical, the velocity required to reach R = 200 km is v ~600 m/s; both values are well below Pluto's escape velocity of 1212 m/s.

Accordingly,we conclude that for reasonable ejection velocities and the observed horizontal extent of the putative cryoclasic deposits, the fountaining model suits the observations best.

6. Alternatives to the cryovolcanism scenario

The case for cryovolcanic activity in the Virgil Fossae region rests on 1) the spatial coincidence of an exposure of H_2O ice that carries a distinctive red chromophore and the spectroscopic signature of an ammoniated compound, 2) morphological characteristics of fluid debouchment along a fault and an airborne deposit of cryoclastics, and 3) occurrence in a zone deeply fractured by crustal extension. Here we consider possible alternative explanations to account for the observations.

In terms of morphology, it is possible that the surface and small craters near Virgil Fossae (e.g., Fig. 3a) are topographically muted (mantled) by the fallout and accumulation of large amounts of tholins produced in the atmosphere. Tholin dust may have aggregated to form particles that saltated by winds to produce a particularly thick mantle near the south rim of the fossae. Or, these small pit craters on the south rim of the main trough are ancient and have been degraded by smaller impacts and/or ground shaking during the formation of Virgil Fossae. The redistribution of tholins from the atmosphere by surface winds in a previous epoch might account for the current pattern of some of the distinctive red material, but does not readily explain its occurrence along the inner face of the south wall of the main trough shown in Figures 4a and 7b.

Water ice is acknowledged to be the bedrock of much of Pluto's exposed crust, and most exposures are colored by red-orange chromophores. The detection of the ammonia signature in the H_2O ice exposed in and around Virgil Fossae adds a dimension to the composition and geological history of this particular region. The exposures of distinctively colored H_2O ice with its ammonia signature in the Virgil trough could represent landslips from the steep walls. While mass wasting from the walls is a likely

occurrence, it is not clear how the entire H_2O ice exposure could acquire the uniformity of color it exhibits unless the entire ice column carries the chromophore. The uniformity of color and coverage supports the view that the distinctive color at this location represents a coating of ice from another source, and that it is not a separate component that precipitated from the atmosphere.

Current glacial activity is seen in the eastern margins of Sputnik Planitia and within the planitia itself. It may be possible that a glacial mantle composed of volatile ices (N_2, CO, CH_4) once covered H_2O bedrock over the large region west of Sputnik Planitia. There is no evidence of scouring by the movement of such an ice pack, but if it left behind a mantle of particulates as it evaporated during some climatic episode, the muted terrain and its spatial distribution might be explained. However, because the muted terrain itself consists of H_2O ice, this scenario seems unlikely.

In summary, there appears to be no clear and plausible single alternative to the cryovolcanic hypothesis put forward in this paper that explain all the observed compositional and morphological characteristics of the Virgil Fossae region.

7. Conclusions and main points

Images and spectral data of the Virgil Fossae region of Pluto obtained with the New Horizons spacecraft in 2015 provide evidence for geologically recent cryovolcanic activity in fossae troughs and the surrounding terrain. Virgil Fossae is a graben complex formed by extensional tectonism in the broader geophysical setting of a stressed annulus surrounding the basin containing the nitrogen ice mass of Sputnik Planitia. The spectral data show the presence of H_2O ice that also carries the spectral signature of NH_3, probably in the form of a hydrate or ammoniated salts. The ammoniated H_2O is tinted with a distinctive red-orange colorant that is likely to be a complex macromolecular organic tholin. The data and observations presented in this paper on the distribution of the H_2O bearing the ammonia signature and the red coloration support the contention that the fault constituting the south wall of the main trough of the graben provided a conduit from a subsurface fluid reservoir to the surface where an eruption occurred along the ~300-km length of the wall. The greatest volume was emitted from a vent or vents in the western part of the main trough, where the cryolava accumulated, freezing as it reached the surface. In the same region, one or more vents erupted as a fountain, dispersing a cryoclastic blanket of presumably frozen particulates that extends some 200 km from the source and covers an area ~200 x 300 km in size. There are several examples of muted topography (troughs and craters) within ~50 km of the putative main vent, suggestive of a blanket of unknown thickness deposited by the fountain. It is in this same region where the H_2O ice spectral signature is strongest.

The molecular structure of ammonia as an ice, as a hydrate, and as a salt is susceptible to destruction by elements of the space environment that include ultraviolet photons, and charged atomic particles in the solar wind and from the Galaxy (GCR). Ammoniated salts and minerals appear to be more robust against such destruction, but reliable quantitative data are apparently not available. The ultraviolet Lyman-α flux from the Sun

and the interplanetary medium incident on Pluto's surface is moderated by CH_4 in the atmosphere, which according to models, permits between ~0.01% and 10% penetration over annual and millennial timescales. The incident flux of solar wind particles on the surface is unknown because much of the flux from the Sun is diverted through interactions with Pluto's extended atmosphere. In any case, both the UV and solar wind flux affect only the uppermost several micrometers of the surface, which is the optical penetration depth for the remote sensing observations that reveal the NH_3 and H_2O infrared spectral signatures. Mechanical gardening of the surface and the diffusive migration of subsurface NH_3 into the H_2O ice may account for the persistence of the spectral signature in the face of its destruction. The NH_3 in the uppermost meter of Pluto's icy surface is subject to destruction by GCR on the timescale of ~10^9 y, and might therefore serve to limit the quantity of NH_3 available for diffusive migration through H_2O to the visible surface.

The distinctive red-orange color seen in Virgil Fossae and surroundings is spatially coincident with the exposures of H_2O ice with the ammonia spectral signature described here, showing that the coloring agent is a component of the ice, suggesting that they were emplaced contemporaneously. The coloring agent may be a macromolecular organic component of the fluid NH_3-H_2O that erupted onto the surface, resulting from chemical reactions with native organic materials in the solar nebula accreted by Pluto during its formation. Alternatively, it may have originated within the fluid from chemical reactions of ammoniated water with minerals comprising Pluto's rocky component, which is presumed to be of chondritic composition.

There is no direct spectroscopic evidence for the composition of the red material in this region or elsewhere on Pluto, but we note that in tholins made in the laboratory, diagnostic bands in the region of the spectrum available in the LEISA data are very weak and in any event are indicative only of major functional groups common to a vast number of organic chemicals. Tholins made by UV and charged-particle irradiation of a mixture of N_2, CH_4, and CO ices, as found on Pluto, produced a refractory and strongly colored residue (Materese et al. 2014, 2015; see also Baratta et al. 2015).

The large-scale geophysical setting of Virgil Fossae and other tectonic structures in the western part of an arc centered on Sputnik Planitia appears to be conducive to the cryovolcanism interpretation of the structure and other characteristics of Virgil Fossae and its surroundings proposed here. Stress induced by the freezing of a subsurface liquid H_2O layer, true polar wander, and loading of the basin containing the Sputnik Planitia nitrogen sea, promoted fracturing in the lithosphere, resulting in Virgil Fossae and similar structures. Deep faulting in Virgil Fossae and surrounding structures tapped into a subsurface fluid reservoir, providing a route for the escape of the fluid, pressurized by gas or tectonic stress on the reservoir. The fluid was ejected both as a cryoflow and a fountain, but the flow was inhibited by rapid freezing, while the fountain deposited a blanket of colored, ammoniated H_2O icy particles over several hundred square kilometers.

ACKNOWLEDGMENTS

We thank Drs. Luis Teodoro for helpful discussions about GCR penetration in ices, Francis Nimmo on the dispersal of cryoclastics, and Ted Roush for advice on the spectra of ammoniated salts. We thank two anonymous referees for their careful reading and thoughtful comments that led to improvements in this paper. Spectra of ammoniated salts were found in the Brown University RELAB data base. This work is supported primarily by NASA's New Horizons project.

REFERENCES

Agostinelli, S., Allison, J., Amako, K. et al. 2003. GEANT4—a simulation toolkit. Nucl. Instrum. Methods Phys. Res. Sect. A. 506, 250-303.

Allamandola, L. J., Sandford, S. A., & Valero, G. 1988. Photochemical and thermal evolution of interstellar/pre-cometary ice analogs. Icarus 76, 225-252.

Atri, D. 2016. On the possibility of galactic cosmic ray-induced radiolysis-powered life in subsurface environments in the Universe. J. Royal Soc. Interface 13.123: 20160459.

Baratta, G., Chaput, D., Cottin, H. et al. 2015. Organic samples produced by ion bombardment of ices for the EXPOSE-R2 mission on the International Space Station. Planet. Space Sci. 118, 211-220

Bennett, C. J. Pirim, C., Orlando, T. M. 2013. Space-weathering of solar system bodies: A laboratory perspective. Chem. Rev. 113, 9086-9150.

Berg, B. L., Cloutis, E. A., Beck, P., et al. 2016. Reflectance spectroscopy (0.35-8μm) of ammonium-bearing minerals and qualitative comparison to Ceres-like asteroids. Icarus 265, 218-237.

Bernstein , M. P., Sandford , S. A., and Allamandola, L. J. 2000. H, C, N, and O isotopic substitution studies of the 2165 wavenumber (4.62 micron) “XCN” Feature produced by ultraviolet photolysis of mixed molecular ices. Astrophys. J. 542, 894-897

Bertrand, T., Forget, F, Umurhan, O. M. et al. 2019. The methane cycles on Pluto over seasonal and astronomical timescales. Icarus (in press).

Caine, J.S., Evans, J.P., Forster, C.B. 1996. Fault zone architecture and permeability structure. Geology, 24, 11, doi: 10.1130/0091-7613(1996)024<1025:FZAAPS>2.3.CO;2.

Cook, J. C., Dalle Ore, C. M., Protopapa, S., Binzel, R. P., Cartwright, R., Cruikshank, D. P., Earle, A., Grundy, W. M., Ennico, K., Howett, C., Jennings, D. E., Lunsford, A. W., Olkin, C. B., Parker, A. H., Philippe, S., Reuter, D., Schmitt, B., Stansberry, J. A., Stern, S. A., Verbiscer, A., Weaver, H. A., Young, L. A. 2018. Composition of Pluto’s small satellites: Analysis of New Horizons spectral images. Icarus 315, 30-45.

Cruikshank, D. P., Imanaka, H., and Dalle Ore, C. M. 2005. Tholins as coloring agents on outer Solar System bodies. Adv. Space Res. 36, 178-183.

Cruikshank, D. P., Materese, C. K., Pendleton, Y. J. et al. 2019. Prebiotic chemistry of Pluto. Astrobiology 17, issue 7.

Dalle Ore, C. M., Cruikshank, D. P., Protopapa, S. et al. 2019. Detection of ammonia on Pluto's surface in a region of geologically recent tectonism. Science Advances (in press).

Dartnell, L. R., Desorgher, L., Ward, J. M., Coates, A. J. 2007. Modeling the surface and subsurface martian radiation environment: implications for astrobiology." Geophys. Res. Lett. 34, L02207 (6 pp).

Demyk, K., Dartois, E., d'Hendecourt, L. B., Jourdain De Muizon, M., Heras, A. M., Breitfellner, M. 1998. Laboratory identification of the 4.62-μm solid state absorption band in the ISO-SWS spectrum of AFGRL 7009S. Astron. & Astrophys. 339, 553

DeSanctis, M. C., Ammannito, E., Raponi, A. et al. 2015. Ammoniated phyllosilicates with a likely outer Solar System origin on (1) Ceres. Nature 528, 241-244. doi:10.1038/nature16172

DeSanctis, M. C., Raponi, A., Ammannito, E. et al. 2016. Bright carbonate deposits as evidence of aqueous alteration on (1) Ceres. Nature 536, 54-57. doi: 10.1038/nature18290

Earle, A. M., Binzel, R. P., Young, L. A. et al. 2017. Long-term surface temperature modeling of Pluto. Icarus 287, 37-46.

Fagents, S. A. 2003. Considerations for effusive cryovolcanism on Europa: The post-Galileo perspective. J. Geophys. Res. 108, No. E12, doi:10.1029/2003JE002128.

Gladstone, G. R. Pryor, W. R., Stern, S. A., Ennico, K., Olkin, C. B., Spencer, J. R., Weaver, H. A., Young, L. A., Bagenal, F., Cheng, a. F., Cunningham, N. J., Elliott, H. A., Greathouse, T. K., Hinson, D. P., Kammer, J. A., Linscott, I. R., Parker, J. Wm., Retherford, K. D., Steffl, A. J., Strobel, D. F., Summers, M. E., Throop, H., Versteeg, M. H., Davis, M. W. 2018. The Lyman-α sky background as observed by New Horizons. Geophys. Res. Lett. 10.1029/2018GL078808.

Grim, R. J. A., and Greenberg, J. M. 1987. Ions in grain mantles - The 4.62 micron absorption by OCN^- in W33A. Astrophys. J. 321, L91-L96.

Grundy, W. M., Binzel, R. P., Buratti, B. J., Cook, J. C., Cruikshank, D. P., Dalle Ore, C. M., Earle, A. M., Ennico, K., Howett, C. J. A., Lunsford, A. W., Olkin, C. B., Parker, A. H., Philippe, S., Protopapa, S., Quirico, E.,Reuter, D. C., Schmitt, B., Singer, K. N., Verbiscer, A. J., Beyer, R. A., Buie, M. W., Cheng, A. F., Jennings, D. E., Linscott, I. R., Parker, J. Wm., Schenk, P. M., Spencer, J. R., Stansberry, J. A., Stern, S. A., Throop, H.

B., Tsang, C. C. C., Weaver, H. A., Weigle, G. E. II, Young, L. A., and the New Horizons Science Team. 2016a. Surface compositions across Pluto and Charon. Science 351, issue 6279, aad9189-8.

Grundy, W. M., Cruikshank, D. P., Gladstone, G. R., Howett, C. J. A., Lauer, T. R., Spencer, J. R., Summers, M. E., Buie, M. W., Earle, A. M., Ennico, K., Parker, J. Wm., Porter, S. B., Singer, K. N., Stern, S. A., Verbiscer, A. J., Beyer, R. A., Binzel, R. P., Buratti, B. J., Cook, J. C., Dalle Ore, C. M., Olkin, C. B., Parker, A. H., Protopapa, S., Quirico, E., Retherford, K., D., Robbins, S. J., Schmitt, B., Stansberry, J. A., Umurhan, O. M., Weaver, H. A., Young, L. A., Zangari, A. M., Bray, V. J., Cheng, A. F., McKinnon, W. B., McNutt, R. L., Moore, J. M., Reuter, D. C., Schenk, P. M., and the New Horizons Science Team 2016b. Formation of Charon's red polar caps. Nature 539, 65-68 +online supplementary material.

Grundy, W., Bertrand, T., Binzel, R. P., Buie, M. W., Buratti, B. J., Cheng, A. F., Cook, J.C., Cruikshank, D. P., Devins, S. L., Dalle Ore, C. M., Earle, A. M., Ennico, K., Forget, F., Gao, P., Gladstone, G. R., Howett, C. J. A., Jennings, D. E., Kammer, J. A., Lauer, T. R., Linscott, I. R., Lisse, C. M., Lunsford, A. W., McKinnon, W. B., Olkin, C. B., Parker, A. H., Protopapa, S., Quirico, E., Reuter, D. C., Schmitt, B., Singer, K., N., Spencer, J., A., Stern, S. A., Strobel, D. F., Summers, M. E.,Weaver, H., A., Weigle, G. E. II, Wong, M. L., Young, E. F., Young, L. A., Zhang, X. 2018. Pluto's haze as a geological material. Icarus 314, 232-245.

Hammond, N. P., Barr, A. C., Parmentier, E. M. 2016. Recent tectonic activity on Pluto driven by phase changes in the ice shell. Geophys. Res. Lett. 10.1002/2016GL069220.

Hammond, N. P., Parmentier, E. M., Barr, A. C. 2018. Compaction and melt transport in ammonia-rich ice shells: Implications for the evolution of Triton. J. Geophys. Res. Planets. doi:10.1029/2018JE005781.

Hansen, C. J., Shemansky, D. E., Esposito, L. W., Steward, A., I. F., Lewis, B. >R., Colwell, J. E., Hendrix, A. R., West, R. A., Wait, J. H. Jr., Teolis, B., Magee, B. A. 2011. The composition and structure of the Enceladus plume. Geophys. Res. Lett. 38, L11202. doi:10.1029/2011GL047415.

Hanna, J.C., Phillips, R.J. 2006. Tectonic pressurization of aquifers in the formation of Mangala and Athabasca Valles, Mars. J. Geophys. Res. 111, E03003, doi: 10.1029/2005JE002546.

Holler, B. J., Young, L. A., Buie, M. W., Grundy, W. M., Lyke, J. E., Young, E. F., Roe, H. G. 2017. Measuring temperature and ammonia hydrate ice on Charon in 2015 from Keck/OSIRIS spectra. Icarus 284, 394-406.

Howard, A. D., Moore, J. M., Umurhan, O. M., White, O. L., Anderson, R. S., McKinnon, W. B., Spencer, J. R., Schenk, P. M., Beyer, R. A., Stern, S. A., Ennico, K., Olkin, C. B.,

Weaver, H. A., Young, L. A., New Horizons Science Team. 2017. Present and past glaciation on Pluto. Icarus 287, 287-300.

Hsu, H.-W., Postberg, F., Yasuhito, S., Takazo, S., Kempf, S. et al. 2015. Ongoing hydrothermal activities within Enceladus. Nature 519, 207-209. DOI: 10.1038/nature14262.

Hudson, R. L., Palumbo, M. E., Strazzulla, G., Moore, M. H., Cooper, J. F., Sturner, S. J. 2008. Laboratory studies of the chemistry of transneptunian object surface materials. In The Solar System Beyond Neptune (M. A. Barucci, H. Boehnhardt, D. P. Cruikshank, A. Morbidelli, Eds. Univ. Arizona Press pp. 507-523.

Imanaka, H., Khare, B. N., Elsila, J. E., Bakes, E. L. O., McKay, C. P., Cruikshank, D. P., Sugita, S., Matsui, T., and Zare, R. N. 2004. Laboratory experiments of Titan tholin formed in cold plasma at various pressures: Implications for nitrogen-containing polycyclic aromatic compounds in Titan haze. Icarus 168, 344-366.

Kargel, J. S., Croft, S. K., Lunine, J. I., Lewis, J. S. 1991. Rheological poroperties of ammonia-water liquids and crystal-liquid slurries: Planetological applications. Icarus 89, 93-112.

Kim, Y.-S., Peacock, D. C. P., Sanderson, D. J. 2004. Fault damage zones. J. Structural Geol., 26, 3, 503-517, doi: 10.1016/j.jsg.2003.08.002.

Keane, J. T., Matsuyama, I., Kamata, S., Steckloff, J. K. 2016. Reorientation and faulting of Pluto due to volatile loading within Sputnik Planitia. Nature 540, 90-93.

Kebukawa, Y., Chan, Q. H. S., Tachibana, S., Kobayashi, K., Zolensky, M. E. 2017. One-pot synthesis of amino acid precursors with insoluble organic matter in planetesimals with aqueous activity. Sci. Adv. 3:e1602093, 17 March.

Lesage, E., Massol, H., Schmidt, F. 2018. Cryomagma ascent on Europa. https://arxiv.org/pdf/1804.00890.pdf

Livingston, F. E., Smith, J. A., George, S. M. 2002. General trends for bulk diffusion in ice and surface diffusion on ice. J. Phys. Chem. A 106, 6309-6318.

Loeffler, M. J., Raut, U., Baragiola, R. A. 2010a. Radiation chemistry in ammonia-water ices. J. Chem. Phys. 132, 054508

Loeffler, M. J., Baragiola, R. A. 2010b. Photolysis of solid NH_3 and NH_3–H_2O mixtures at 193 nm. J. Chem. Phys. 133, 214506.

Manga, M., Wang, C. -Y. 2007. Pressurized oceans and the eruption of liquid water on Europa and Enceladus. Geophy. Res. Lett. 34, L07202, doi:10.1029/2007/GL029297.

Materese, C. K., Nuevo, M., Sandford, S. A. 2014. N- and O-heterocycles produced from the irradiation of benzene and naphthalene in H_2O/NH_3-containing Ices. Astrophys. J. 800:116 (8pp).

Materese, C. K., Cruikshank, D. P., Sandford, S. A.,Imanaka, H., Nuevo, M. 2015. Ice chemistry on outer solar system bodies: Electron radiolysis of N_2-, CH_4-, and CO-containing ices. Astrophys. J. 812:150 (9pp). October 20.

McComas, D. J., Elliott, H. A., Weidner, S., et al. 2016. Pluto's interaction with the solar wind. J. Geophys. Res. Space Phys. 121, 4232-4246. doi10.1002/2016JA022599.

McKinnon, W. B., Stern, S. A., Weaver, H. A., Nimmo, F., Bierson, C. J., Cook, J. C., Grundy, W. M., Cruikshank, D. P., Parker, A. H., Moore, J. M., Spencer, J. R., Young, L. A., Olkin, C. B., Ennico Smith, K. 2017. Origin of the Pluto-Charon system: Constraints from the New Horizons flyby. Icarus 287, 2-11.

Moore, M. H., Ferrante, R. F., Hudson, R. L., Stone, J. N. 2007. Ammonia–water ice laboratory studies relevant to outer Solar System Surfaces. Icarus 190, 260-273.

Moore, J. M., McKinnon, W. B., Spencer, J. R., Howard, A. D., Schenk, P. M., Beyer, R. A., Nimmo, F., Singer, K. N., Umurhan, O. M., White, O. L., Stern, S. A., Ennico, K., Olkin, C. B., Weaver, H. A., Young, L. A., Binzel, R. P., Buie, M. W., Buratti, B. J., Cheng, A. F., Cruikshank, D. P., Grundy, W. M., Linscott, I. R., Reitsema, H. J., Reuter, D. C., Showalter, M. R., Bray, V. L., Chavez, C. L., Howett, C. J. A., Lauer, T., R., Lisse, C. M., Parker, A. H., Porter, S. B., Robbins, S. J., Runyon, K., Stryk, T., Throop, H. B., Tsang, C. C. C., Verbiscer, A. J., Zangari, A. M., Chaikin, A. L., Wilhelms, D. E., and the New Horizons Science Team. 2016. The geology of Pluto and Charon through the eyes of New Horizons. Science 351, 1284-1293, issue 6279, aad7055.

Neveu, M., Desch, S. J., Shock, E. L., Glein, C. R. 2015., Prerequisites for explosive cryovolcanism on dwarf planet-class Kuiper belt objects. Icarus 246, 48-64.

Neveu, M., Desch, S. J., Castillo-Rogez, J. C. 2017. Aqueous geochemistry in icy world interiors: Equilibrium fluid, rock, and gas compositions, and fate of antifreezes and radionuclides. Geochim. Cosmochim. Acta 212, 324-371.

Nimmo, F., Hamilton, D. P., McKinnon, W. B. et al. 2016. Reorientation of Sputnik Planitia implies a subsurface ocean on Pluto. Nature 540, 94-96.

Nimmo, F., Umurhan, O., Lisse, C. M. et al., 2017. Mean radius and shape of Pluto and Charon from New Horizons images. Icarus. doi: 10.1016/j.icarus.2016.06.027.

Olkin, C. B., Spencer, J. R., Grundy, W. M. et al. 2017. The global color of Pluto from New Horizons. Astron. J. 154, 258 (13pp) December.

Pilling, S., Seperuelo Duarte, E., da Silveira, E. F., Balanzat, E., Rothard, H., Domaracka, A., Boduch, P. 2010. Radiolysis of ammonia-containing ices by energetic, heavy, and highly charged ions inside dense astrophysical environments. Astron. Astrophys. 509, A87 (10 pages).

Pizzarello, S., Cooper, G. W., Flynn, G. J. 2006. The nature and distribution of the organic material in carbonaceous chondrites and interplanetary dust particles. In Meteorites and the Early Solar System, Eds. D. S. Lauretta & H. Y. McSween, Jr., Univ. Arizona Press, pp 625-621.

Postberg, F., Schmidt, J., Hillier, J., Kempf, S., Srama, R. 2011. A salt-water reservoir as the source of a compositionally stratified plume on Enceladus. Nature 74, 620-622. DOI: 10.1038/nature10175

Postberg, F., Khawaja, N., Abel, B., et al. 2018. Macromolecular organic compounds from the depths of Enceladus. Nature doi.org/10.1038/s41586-018-0246-4

Protopapa, S., Grundy, W. M., Reuter, D. C. et al. 2017. Pluto's global surface composition through pixel-by-pixel Hapke modeling of New Horizons Ralph/LEISA data. Icarus 287, 218-228.

Ruesch, O., Platz, T., Schenk, P., McFadden, L. A., Castillo-Rogez, J. C. et al. 2016. Cryovolcanism on Ceres. Science 353. Issue 6303. id.aaf4286.

Robbins, S. J., Singer, K. N., Bray, V. J., et al. 2017. Craters of the Pluto-Charon system. Icarus 287, 187-206.

Roth, L., Saur, J., Retherford, K. D., Strobel, D., Feldman, P. D., McGrath, M., A., Nimmo, F. 2014. Transient water vapor at Europa's south pole. Science 343, 171-174.

Runyon, K. D. 2011. Structural characterization of the Cerberus Fossae and implications for paleodischarge of Athabasca Valles, Mars (Order No. 1500822). Available from ProQuest Dissertations & Theses Global. (900865879). Retrieved from https://search.proquest.com/docview/900865879?accountid=11752

Schenk, P. M., Beyer, R. A., McKinnon, W. B., Moore, J. M., Spencer, J. R., White, O. L., Singer, K., Nimmo, F., thomason, C., Lauer, T. R., Robbins, S., Umurhan, O. M., Grundy, W. M., Stern, S. A., Weaver, H. A., Young, L. A., Ennico Smith, K., Olkin, C., and the New Horizons team. 2018. Basin, fractures and volcanoes: Global cartography and topography of Pluto from New Horizons. Icarus 314, 400-433.

Schmitt, B., Philippe, S., Grundy, W. M., et al. 2017. Physical state and distribution of materials at the surface of Pluto from New Horizons LEISA imaging spectrometer. Icarus 287, 229-260.

Shock, E. L. 1993. Hydrothermal dehydration of aqueous organic compounds. Geochim. Cosmochim. Acta. 57, 3341-3349

Singer, K. N., White, O. L., Schenk, P. M. et al. 2016. Pluto's putative cryovolcanic constructs. 47th LPSC abstract 2276.pdf.

Singer, K. N., McKinnon, W. B., Gladman, B., Greenstreet, S. et al. 2019. Impact craters on Pluto and Charon indicate a deficit of small Kuiper belt objects. Science 363, 955-959.

Steffl, A. J., Young, L. A., Strobel, D. F. et al. 2019. Pluto's ultraviolet spectrum, surface reflectance, and airglow emissions. Astron. J. (in review).

Stern, S. A., Bagenal, F., Ennico, K. et al. 2015, The Pluto system: Initial results from its exploration by *New Horizons*. Science 350 (issue 6258) pp. 1815-1-8.

Stern, S. A., Binzel, R. P., Earle, A. M., Singer, K. N., Young, L. A., Weaver, H. A., Olkin, C. B., Ennico, K., Moore, J. M., McKinnon, W. B., Spencer, J. R., and the New Horizons Geology, Geophysics and Atmospheres teams. 2017. Past epochs of significantly higher pressure atmospheres on Pluto. Icarus 287, 47-53.

Southworth, B. S., Kempf, S., Schmidt, J. 2015. Modeling Europa's dust plumes. Geophys. Res. Lett. 10.1002/2015GL066502.

Smith, B. A., Soderblom, L. A., Johnson, T. V. et al. 1979. The Jupiter system through the eyes of Voyager 1. Science 204, 951-957.

Sparks, W. B., Schmidt, B. E., McGrath, M. A. et al. 2017. Active cryovolcanism on Europa ? Astrophys. J. Lett. 839, L18 (5 pp) April 20.

Tartèse, R., Chaudisson, M., Gurenko, A., Delarue, F., Robert, F. 2018. Insights into the origin of carbonaceous chondrite organics from their triple oxygen isotope composition. PNAS, doi/10.1073/pnas.1808101115.

Tian, F., Stewart, A. I. F., Toon, O. B., Larsen, K. W., Esposito, L. W. 2007. Monte Carlo simulations of the water vapor plumes on Enceladus. Icarus 188, 154-161.

Umurhan, O. M., Howard, A. D., Moore, J. M. et al. 2017. Modeling glacial flow on and onto Pluto's Sputnik Planitia. Icarus 287-301.

Umurhan, O. M. et al. 2019. Recent cryovolcanism in Virgil Fosssae on Pluto: Theoretical considerations. In preparation.

Uras, N., Devlin, J. P. 2000. Rate study of ice particle conversion to ammonia hemihydrate: Hydrate crust nucleation and NH_3 diffusion. J. Phys. Chem. A 104, 5770-5777.

Williams, D. A., Howell, R. R. 2007. Active volcanism: Effusive eruptions. In Io after Galileo, R. M. Lopes and J. R. Spencer, eds. Springer Praxis Books, pp 133-161.

Woodcock, N. H., Fischer, M., 1986. Strike-slip duplexes. J. Structural Geol., 8, 7, 725-735, doi: 10.1016/0191-8141(86)90021-0.

Wooden, D. H., Ishii, H. A., Zolensky, M. E. 2017. Cometary dust: The diversity of primitive refractory grains. Phil. Trans. Royal Soc. A. 375, Issue 2097, id.20160260.

Wyrick, D. Y., Ferrill, D. A., Morris, A. P., Colton, S. L., Sims, D. W. 2004. Distribution, morphology, and origins of Martian pit crater chains. J. Geophys. Res. 109, doi: 10.1029/2004JE002240.
